EUROPEAN COMMISSION

Community Research

SEVENTH FRAMEWORK PROGRAMME

ARCHER

Collaborative Project (CP)

Co-funded by the European Commission under the Euratom Research and Training Programme on Nuclear Energy within the Seventh Framework Programme

Grant Agreement Number : 269892

Start date : 01/02/2011 Duration : 48 Months

www.archer-project.eu

Archer

Advanced Reactor for Cogeneration of Heat & Electricity-R&D

Fabrication reports for CP STRESS Ag and B4C doped coated particles

Authors : LUSTFELD Martin (TUDresden)

ARCHER - Contract Number: 269892
Advanced High-Temperature Reactors for Cogeneration of Heat and Electricity R&D
EC Scientific Officer: Dr. Panagiotis Manolatos

Document title	Fabrication reports for CP STRESS Ag and B4C doped coated particles
Author(s)	LUSTFELD Martin
Number of pages	45
Document type	Deliverable
Work Package	WP 31
Document number	D31.32
Issued by	NRG
Date of completion	17/10/2014
Dissemination level	Confidential, only for members of the consortium (including the Commission Services).

Summary

The pulsed laser deposition process (TU Dresden) was successfully applied to fabricate subsequent coating layers of silver and SiC on spherical ZrO2 kernels with the aim to allow studying silver diffusion through SiC coatings on non-active simulated fuel kernels. The deposition of dense silver coatings that were free of droplets and impurities was accom-plished. However, the subsequent deposition of high quality SiC coatings proved to be challenging. Crack and bubble formation, insufficient crystallinity and non-stoichiometry were issues that required adjustments in the experimental set-up (high vacuum) and an extensive parameter study of the deposition conditions (e.g. pulse frequency and energy, temperature). Ultimately, crack-free and nanocrystalline SiC coatings were successfully deposited onto silver-coated zirconia kernels. Furthermore, in a feasibility study, the PLD process was used to produce B4C coatings both on pure Al2O3 and on TRISO surrogate particles. In the framework of CPStress, such particles should subsequently be coated with state-of-the-art SiC layers and irradiated un-der HTR conditions. Due to neutron absorption, helium will be produced within the B4C layer due to fission of boron producing an internal pressure within the SiC shell. In this manner, the SiC layer strength can be evaluated. Similarly to the fabrication of SiC layers by PLD, the PLD-B4C process was subject to nu-merous iterations until satisfactorily thick, stoichiometric, and crystalline layers could be produced.

Approval

Date	By
17/10/2014	Steven KNOL
06/11/2014	Mathias LAURIE
07/11/2014	Steven KNOL

Distribution list

Name	Organisation	Comments
P. Manolatos	EC DG RTD	Through the EC participant portal
All beneficiaries	ARCHER	Through the private online workspace

ARCHER project – Contract Number: 269892

Advanced High-Temperature Reactors for Cogeneration of Heat and Electricity R&D

EC Scientific Officer: Dr. Panagiotis Manolatos

Document title	Fabrication reports for CP STRESS Ag and B4C doped coated particles
Author(s)	TU Dresden: Anne-Maria Reinecke, Martin Lustfeld, Wolfgang Lippmann
Number of pages	45
Document type	Deliverable
Work Package	WP31
Document number	D31.32-v1
Issued by	TU Dresden
Date of completion	16/10/14
Dissemination level	Restricted to the partners of the ARCHER project

Summary

The pulsed laser deposition process (TU Dresden) was successfully applied to fabricate subsequent coating layers of silver and SiC on spherical ZrO_2 kernels with the aim to allow studying silver diffusion through SiC coatings on non-active simulated fuel kernels. The deposition of dense silver coatings that were free of droplets and impurities was accomplished. However, the subsequent deposition of high quality SiC coatings proved to be challenging. Crack and bubble formation, insufficient crystallinity and non-stoichiometry were issues that required adjustments in the experimental set-up (high vacuum) and an extensive parameter study of the deposition conditions (e.g. pulse frequency and energy, temperature). Ultimately, crack-free and nanocrystalline SiC coatings were successfully deposited onto silver-coated zirconia kernels.

Furthermore, in a feasibility study, the PLD process was used to produce B_4C coatings both on pure Al_2O_3 and on TRISO surrogate particles. In the framework of CPStress, such particles should subsequently be coated with state-of-the-art SiC layers and irradiated under HTR conditions. Due to neutron absorption, helium will be produced within the B_4C

layer due to fission of boron producing an internal pressure within the SiC shell. In this manner, the SiC layer strength can be evaluated.

Similarly to the fabrication of SiC layers by PLD, the PLD-B_4C process was subject to numerous iterations until satisfactorily thick, stoichiometric, and crystalline layers could be produced.

Approval

Rev.	Short description	First author	WP Leader	SP leader	Coordinator
0	First issue	Anne-Maria Reinecke (TU Dresden) 16/10/14	Steven Knol (NRG)	Mathias Laurie (ITU)	Steven Knol ../../..

Distribution list

Name	Organisation	Comments
P. Manolatos	EC DG RTD	
All technical participants	ARCHER	
Steering Committee members	ARCHER	

Table of Contents

Table of Contents 1
1 Introduction 5
2 State of the Art 5
3 Evaluation of Process-Determining Parameters Based on In-House Knowledge of Coating of Planar Substrates 7
3.1 Pulse Energy 7
3.2 Pulse Frequency 8
3.3 Focal Length 9
3.4 Distance Between Target and Substrate 9
3.5 Coating Temperature 10
3.6 Coating Atmosphere 12
4 Experimental 14
4.1 Experimental Setup 14
4.2 Development of Experimental Equipment for PLD Coating of Spherical Substrates 15
4.3 Materials Used 18
5 Results 21
5.1 Coating of ZrO_2 Particles With Silver 21
5.1.1 Coating of ZrO_2 Particles with SiC on Silver at Room Temperature 22
5.1.2 Coating With SiC on Silver in Temperature Range From 350 °C to 800 °C 24
5.1.3 Coating of Silver with SiC in Temperature Range From 800 °C to 1000°C 26
5.2 Coating of Carbon-Covered ZrO_2 Particles with Silver and SiC 29
5.3 Coating of Al_2O_3 Particles with B_4C 31
5.3.1 Effect of Porosity of Target Material on Coating Quality 31
5.3.2 Coating With B_4C at Temperatures of Less Than 300 °C 32
5.3.3 Coating with B_4C at Temperatures of Between 300 °C and 700 °C 35

6 Conclusions..... 38

7 Literature Cited..... 40

1 Introduction

Within the framework of the ARCHER (Advanced High-Temperature Reactors for Cogeneration of Heat and Electricity R&D) EU research program “Fuel and Fuel Cycle” area, a laser-assisted physical coating process for preparing SiC barrier layers and B_4C coatings has been developed and applied to supplement the previously used chemical process of chemical vapor deposition (CVD).

Deliverable 3.1.2 was aimed at performing fundamental investigations on silver and cesium diffusion in TRISO-coated particles. The task of TU Dresden was to prepare silver coatings on spherical Al_2O_3 and ZrO_2 particles by means of pulsed laser deposition (PLD). The spherical particles were supplied by the University of Manchester (UMAN) and, following silver coating at TU Dresden, coated with SiC in a CVD system at UMAN. To prevent premature evaporation of the silver coating during the CVD process, which was carried out at 1600 °C, an additional thin SiC protective layer was applied to the silver coating via PLD.

The objective of deliverable 3.1.3 was to conduct a study on the feasibility of manufacturing a coating system consisting of B_4C and SiC coatings to investigate the mechanical stability of TRISO particles in reactor conditions. Within the irradiation project CPSTRESS, neutron irradiation leads to the occurrence of the fission product helium in the B_4C coatings due to neutron absorption by boron, in turn leading to an overpressure beneath the SiC coating. With knowledge of the mass of boron in the coating and the incident neutron flux as well as the applied coating thickness, the resultant internal pressure can be calculated. Via the failure behavior of the SiC coating, information about the tensile strength of the SiC coatings in irradiated condition can be inferred and various possibilities for optimizing the coating structure design in turn derived from this. The task of TU Dresden was to examine the feasibility of depositing B_4C coatings onto spherical substrates by PLD. Project partner NRG determined the minimum coating thickness required for the process to be 25 µm.

2 State of the art

The pulsed laser deposition (PLD) technology was first used and described in 1965 by Smith and Turner in Rochester, New York, for manufacturing semiconductors and dielectric coatings [1]. The process was characterized by use of a ruby laser, which, unlike the prior process of vapor deposition, enabled material removal via short pulses (≈ 1 µs) as well as free selection of the coating atmosphere by allowing the radiation to be guided

from the outside to the receiver and hence the energy source to be placed outside the deposition chamber. The process only became established in 1987 through the work of T. Venkatesan et al. [2] and the development of excimer lasers with considerably shorter pulse times (20 ns). Vekatesan et al. uncovered a key characteristic of the PLD process: Due to the short pulse time, stoichiometric transfer of the target material to the substrate was possible. In a concrete example, supraconductive coatings from the $YBa_2Cu_3O_{7-\delta}$ system were deposited with the exact same stoichiometry. In subsequent years, the PLD technology started being used for a large number of metals, alloys, and other chemical compounds, including plastics. Because of the relatively high investment costs for the excimer laser system, the application was primarily restricted to high-grade optical coatings and functional coatings such as semiconductor coatings in microelectronics [4][5], multioxide coatings as supraconductors [6], and wear-resistant coatings [7][8][22].

Coatings with silver are made on a large scale using electrochemical methods, sometimes supported by a voltage source. Physical coating methods are primarily used for coatings with functional requirements. For example, sputtering methods are used to apply silver coatings to flat glass in flat glass production plants to enable adjustment of the optical properties, especially reflection. However, in the recent past, PLD systems have been developed, tested, and commercially used to supplant these processes [9][10]. Research has been focused on deposition of silver particles with precisely defined sizes, shapes, and separation distances by PLD [23], with special interest being paid to the differences in optical properties of classic bodies and metal particles that are considerably smaller than the wavelengths of visible light. Especially the sharply delineated absorption bands can be utilized in a multitude of special technological processes [23][24][25][26][27]. Attempts have been made to deposit individual particles, islands, or coatings with thicknesses of a few nanometers. Coatings of thickness greater than 100 nm are used in medical technology, where, for instance, the antibacterial activity of silver is utilized in coatings on medical devices and implants, primarily made of titanium alloys [28][29][30]. Research in this area has centered on surface properties and alloying with additives or the base material. In contrast, large-scale industrial process solutions for plasma coating of spherical particles with silver in vacuum conditions are not known.

Over the last 15 years SiC coatings have been investigated and implemented on single-crystal silicon or on sapphire due to their interesting electronic and electromechanical properties [11][14][15][16][17][18][19][20][21]. Investigations have mainly been centered on particulate-free, homogeneous coatings. The deposition temperature of between 250 °C

and 1100 °C was identified as a key parameter for the resultant coating properties (especially crystal modifications and coating stresses). The coatings were found to exhibit long-range crystalline order starting at a temperature of about 600 °C to 800 °C. Possibilities for reducing stresses, mainly through heat treatment, were also discussed [7][8]. The deposited coatings were less than 500 nm thick in all cases except in the application discussed by Zehnder et al. [11]. In this case, strongly bonded coatings of thickness greater than 5 µm were deposited onto 300-nm-thick silicon substrates and the stresses in the coatings were calculated based on the curvature of the coated sample. There is no information on PLD coatings of SiC on silver in the literature as of yet.

Only in a few cases the PLD of B_4C has been described. Here it should enhance the wear resistant of surfaces instead of favorite boron nitride. The thickness of these layers was in the range of 100 nm up to 1 µm [12][13].

3 Evaluation of process-determining parameters based on in-house knowledge of coating of planar substrates

The quality of the coating deposited onto planar substrates using PLD technology can be affected by a large number of parameters that define the laser beam, the process, and the working environment.

3.1 Pulse energy

Knowing the precise laser energy input over the duration of the process is key to being able to interpret the measurement results. The laser pulse energy measured directly in front of the target was adjusted to a maximum value of 410 mJ. Laser beam irradiation of a target with an area of 1.5 x 1.3 mm² yielded a maximum homogeneous energy density of 20 J/cm², much greater than the SiC ablation threshold of approx. 1 J/cm² [16]. This pulse energy is only available at the beginning of a coating test. The setup with the target at a 45° angle to the laser beam used in this work caused secondary coating of the coupling window and hence a reduction in the window transmission. This effect was investigated within the scope of this work and is illustrated in Figure 1 in the form of the results of 22 tests. According to the results, for a total energy input of 50 kJ, the pulse energy drops by up to 50% during the coating test. On the other hand, ablation at low pulse energy can

lead to “window cleaning effects,” providing an explanation for the occurrence of the two negative values.

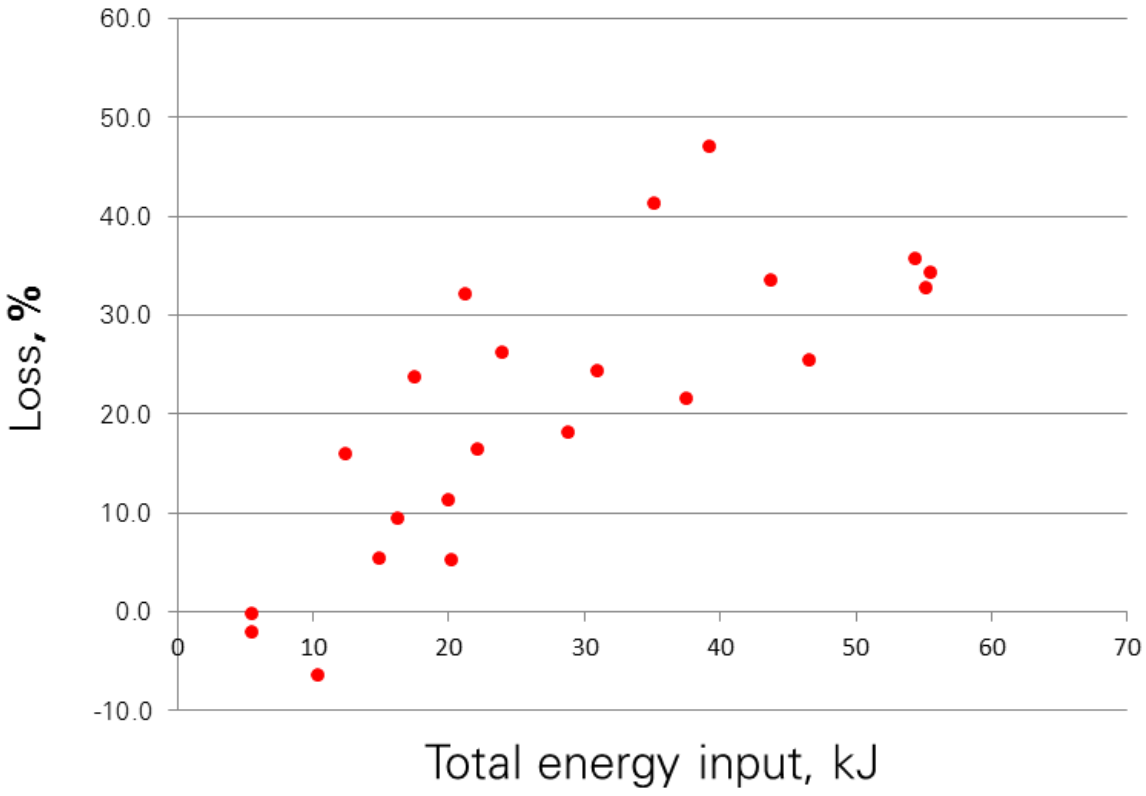


Figure 1: Loss of laser beam energy as a function of total energy input for one coating cycle

The amplitude of the pulse energy directly affected the deposition rate, a main factor characterizing the effectiveness of the process in terms of the coating thickness in relation to the coating time. Deposition rates of up to 8 nm/s were achieved.

3.2 Pulse frequency

The pulse frequency can be varied from 1 Hz to 40 Hz. It affects the deposition rate (the coating growth rate is proportional to the number of pulses per second) and the degree of pulse overlapping on the target, which also depends on the rotational speed of the target.

Pulse frequency and rotational speed of the target were selected to minimize pulse overlapping (Figure 2). The greater the amount of pulse overlapping, the higher the specific heat input into the target. This can force the formation of a melt or spalling, in which particles are detached from the target due to recoil forces and are deposited unintendedly in the form of droplets or particulates onto the substrate.

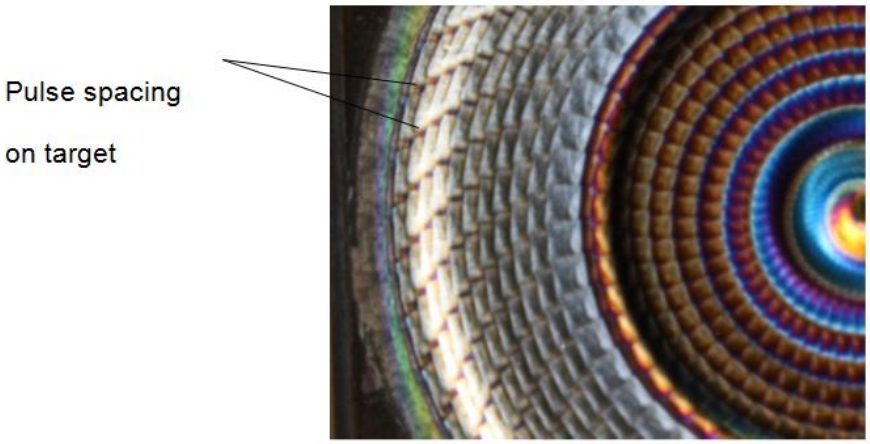


Figure 2: Arrangement of laser pulses on target, influenced by pulse frequency and nonlinear rotational speed

3.3 Focal length

The correct name for the smallest attainable spot after the focusing optics in an excimer laser is not the “focus,” but rather a “projection.” This is based on the way in which the beam is generated and the optics used for beam shaping. Ablation with a defocused laser beam is not recommended because an inhomogeneous intensity profile prevails under these conditions. The projected image of the laser beam described a rectangle with dimensions of approximately 1.5 x 1.3 mm². The focusing optics had a focal length of 400 mm.

3.4 Distance between target and substrate

The target and the substrate are aligned parallelly. By varying the distance between substrate and coating, the kinetic energy of the ablated particles impinging on the substrate can be adjusted as well as the mean coating thickness, and the coating thickness distribution on the substrate. At the time of ablation, the components of the target (atoms, ions, and electrons) are accelerated in a direction normal to the target by expansion of the plasma and decelerated on their way to the substrate by collisions with each other due to their different speeds or with components of the working atmosphere. Hence, the particles are first accelerated after exiting the target and then decelerated more and more as they approach the substrate as a function of the vacuum properties. The kinetic energy of the impinging particles can be so high that coating deposition is made impossible by the superimposed sputter effect. Due to the limitations imposed by the construction, the target-to-substrate spacing could be varied in the range between 30 mm and 70 mm. Based on recommendations given in the literature, a spacing of 40 mm was selected.

Figure 3 shows an example of a coating thickness distribution across the coating cross section on a flat plate for two different pulse energies. The coating thickness was measured on the fracture surface with the help of a 3D laser scanning microscope (LSM) of type Keyence VK 9700. The widely distributed coating thickness, which showed a maximum in the region of the target normal, could be attributed to the quasi-pointwise particle emission from the target. Furthermore, the influence of the pulse energy on the ablation direction is made evident by the different slopes of the two curves. In the test setup used in this work, the spheres to be coated are located on a circular area of diameter 20 mm at a distance of 40 mm from the target. They exhibit an ablation angle of 30° in with respect to the target normal, achieving the maximum coating rate with largely homogeneous coating of the moving spheres.

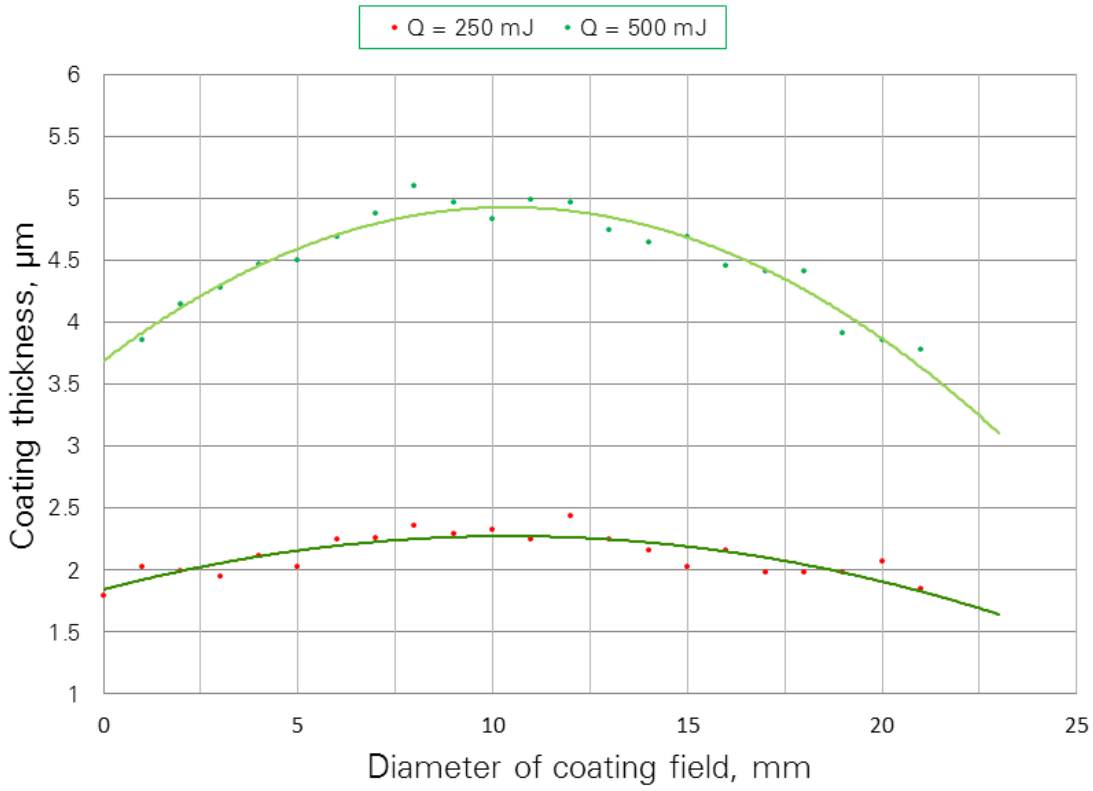


Figure 3: Change in coating thickness over the area of a planar substrate as a function of pulse energy for a spacing of 40 mm between target and substrate

3.5 Coating temperature

The temperature of the samples to be coated was adjusted by means of a 3 kW diode laser and could be varied freely over a wide range. With silver, a common coating material for mirrors, the absorption of this laser radiation of wavelength 808 nm is limited to about 3% [38]. In contrast, SiC absorbs the laser radiation with an efficiency of greater than 99%

[39]. For B_4C, a similarly high absorption can be expected. Unlike the noble metal silver, the chemical composition of PLD-SiC and PLD-B_4C, respectively, does not necessarily equal the stoichiometric composition of the target and is a function primarily of the vacuum conditions and the coating temperature. The microstructure of the coatings depends on these parameters as well. It must be assumed that the individual atoms and ions of SiC in the plasma will be deposited independently of each other in case of an unheated substrate. Only starting at a specific substrate temperature it can be expected that chemically bonded SiC with an amorphous structure and possibly free Si and/or C will form. According to the literature, the crystallization temperature of SiC is approximately 800 °C [40]. In fact, the crystallization temperature may vary as a function of the deposition parameters, such as the substrate material and the deposition rate, making it possible for a wide range of crystallization temperatures to be yielded with the PLD technology. In addition, the particle energy and the coating time also affect the coating microstructure (Figure 4 [41]). These parameters can be varied appropriately to obtain the desired crystallite size and shape.

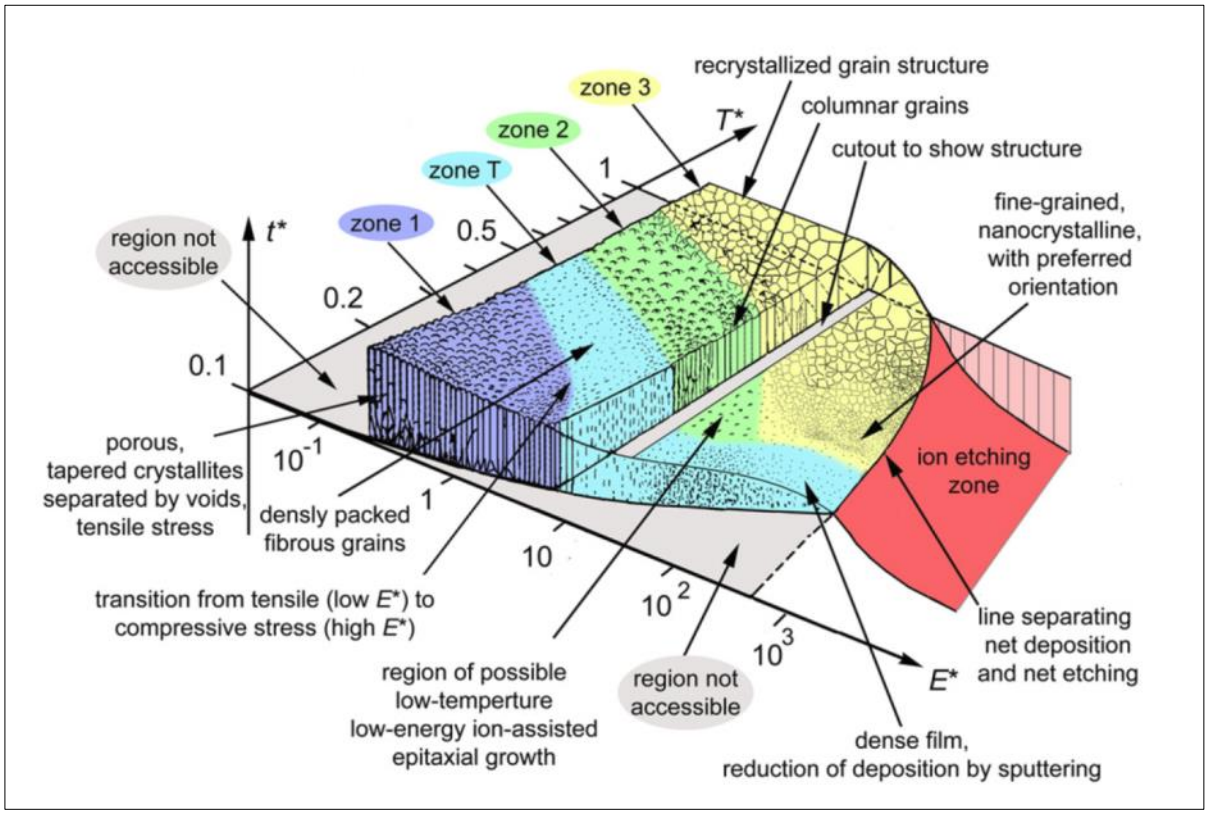


Figure 4: Structure zone diagram [41]. The coating microstructure proved to be dependent on the homologous substrate temperature, the normalized particle energy, and the normalized coating thickness. At a very high particle energy, instead of coating, removal of the substrate surface occurred ("ion etching").

The particles coated within the scope of this work had to be moved constantly during the coating process, which took place in a vacuum, in order for a uniform coating structure to be achieved over the entire particle surface. This made temperature measurement even more difficult. The only possibility was via contactless measurement through a window in the vacuum chamber. In this work, the measurement was carried out using an infrared camera, which was installed at a distance to the object of about 40 cm. With a resolution of 1280 x 960 pixels and an image field of 160 x 120 mm², each particle was represented only by 4 x 4 pixels (Figure 5). Movement of the particles during measurement resulted in large uncertainties, which, however, could be reduced through measurement of the temperature right after the spheres came to a standstill.

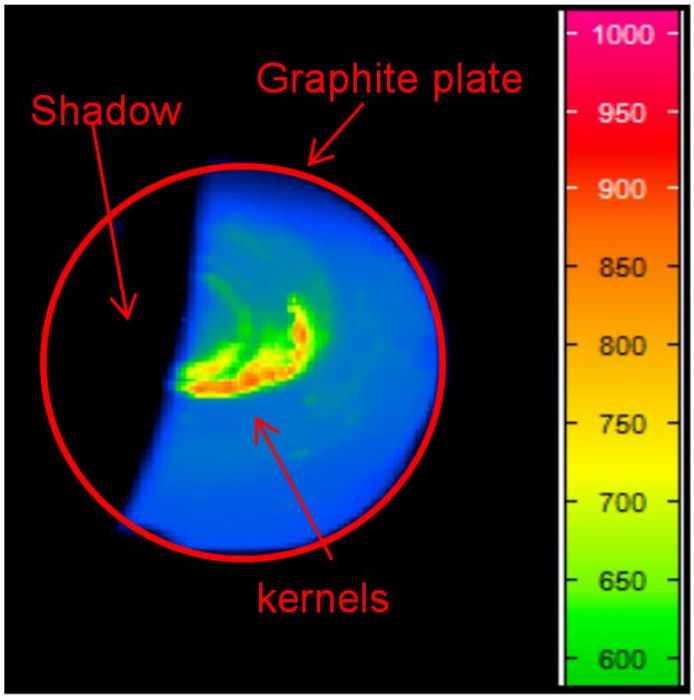


Figure 5: Thermogram of heated spheres at standstill, Tmax = 980 °C

3.6 Coating atmosphere

The PLD process was performed in a vacuum, primarily to ensure unimpeded spreading of the target components and avoidance of interactions with other elements between the target and the substrate. In the vacuum chamber used, a high vacuum of 10^{-4} mbar was generated. This reduced the number of species from 10^{19} cm^{-3} at normal pressure to 10^{12} cm^{-3} under vacuum conditions. Both the melting and boiling temperatures of elements and compounds depend on the pressure of the surrounding atmosphere. If crystalline SiC is deposited onto a silver coating at the necessary deposition temperature of > 800 °C, it must be ensured that the temperature-dependent partial pressure of silver [42] does not

get too high (Figure 6). To accomplish this, the pressure in the vacuum chamber can be increased accordingly. In the experiment, a pressure of 2.5 x 10^{-1} mbar was hence chosen when crystalline SiC was to be deposited onto silver. However, this change in pressure immediately resulted in an increase in particle density to approx. 10^{15} cm^{-3} and hence a reduction in the mean free path from 10 m at 10^{-4} mbar to 10 mm at 10^{-1} mbar. Not only did the probability of collisions increase, but the probability of contamination of the coating by incorporation of oxygen and nitrogen as main components of the air also increased. Purging the chamber with an inert gas (Ar in this case) can counteract the chemical reaction, but a change in the stoichiometry of the coating composition can then be expected. The reason for this is the fact that the cross section of argon atoms is nearly three times that of oxygen or nitrogen atoms, which increases the probability of collision of the gas atoms with the relatively large Si ions.

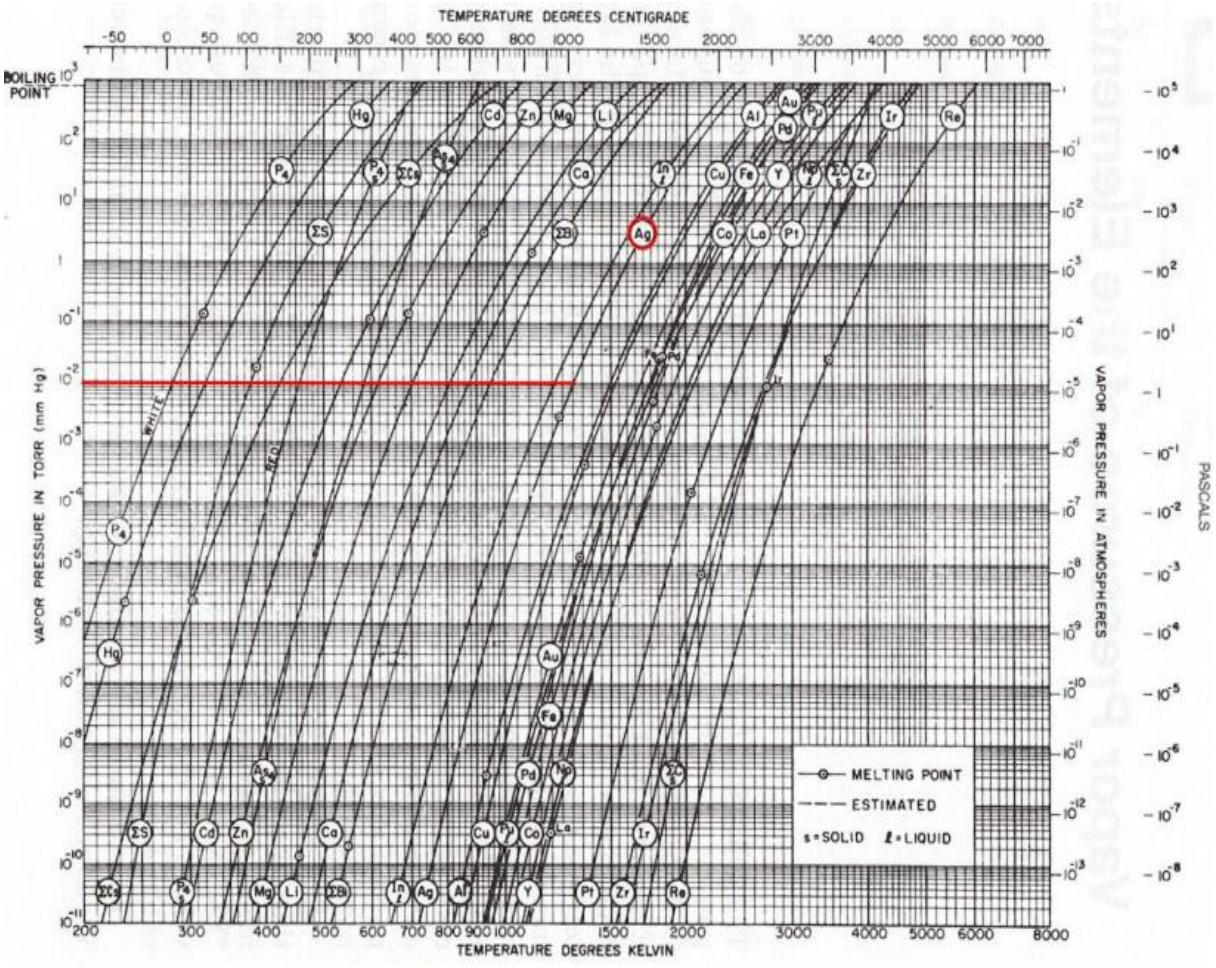


Figure 6: Dependence of vapor pressure on temperature for selected elements [42]

4 Experimental

4.1 Experimental setup

For generation of silver and SiC coatings on the spheres, a PLD test system using an excimer laser unit for ablation of the coating material was installed. A Coherent LPX Pro 305i excimer laser with a wavelength of 248 nm, a pulse duration of 25 ns, and a pulse repetition frequency of 40 Hz was used. The wavelength of the laser pulses in the UV range ensured the ablation of material required in the PLD process by explosive evaporation with a very small heat-affected zone. The laser had a maximum pulse energy of 1.1 J, yielding a laser fluence of 20 J/cm² for a focused laser beam cross-sectional area of about 5 mm². According to Reitano et al. [34], the ablation threshold for SiC is 1.1 J/cm².

A diode laser beam with a wavelength of 808 nm was also directed at the moving spheres to heat them up to the required substrate temperature. The wavelength of 808 nm and the selected laser power ensured that the energy input by the diode laser did not reach the ablation threshold of SiC.

A high-vacuum chamber with a capacity of 0.03 m³ housed the coating equipment as the receiver for the PLD process. Unless otherwise stated, the tests were conducted in a high vacuum of $< 9*10^{-4}$ mbar. A total of four optical windows were provided, one for transmission of the excimer laser radiation to the target, one for transmission of the diode laser radiation to the spheres to heat them up, one for recording of the sample temperature via the infrared camera, and one enabling observation of the process. The windows were made of quartz glass or zinc selenide glass according to the wavelengths to the transmitted. Through-holes were provided for chamber evacuation, power supply to and cooling of motors, and transmission of rotation to the target holder. A schematic diagram of the working chamber showing the test setup is given in Figure 7.

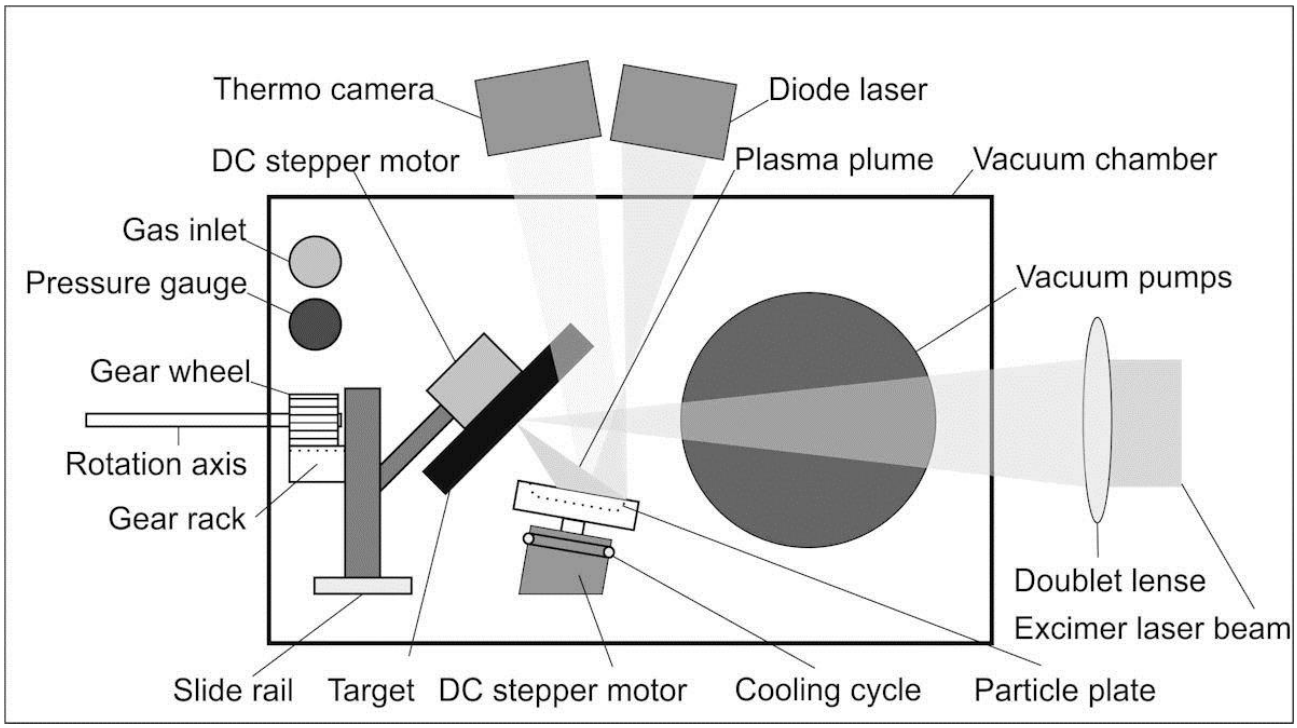


Figure 7: Schematic diagram of working chamber test setup

A holder enabling fixation as well as translational and rotational movement of the target relative to the excimer laser beam via a stepper motor was installed in the vacuum chamber. Uniform surface removal of the target at an angle of 30° to 60° to the beam axis was achieved by sliding of the unit along a rail. With control of the rotation with variable speed and simultaneous superimposition of the constant rotational speed of the vacuum-grade stepper motor (to 10^{-4} mbar) from Phytron, the laser beam described a spiral path on the surface of the target, enabling uniform removal of the target surface at a constant laser pulse frequency.

4.2 Development of experimental equipment for PLD coating of spherical substrates

Apart from suitable laser and operating parameters, uniform and complete rotation of the spherical substrates (“kernels”) during the coating process is crucial for a good coating quality. Vacuum-grade, temperature-resistant, durable components that allow for continuous coating of the spheres without any shadowing of the plasma plume are required to ensure a high, uniform deposition rate. In the CVD (chemical vapor deposition) method conventionally used for coating of spherical nuclear fuel, uniform coating is achieved through a fluidized bed generated by a gas flow [31][32][33]. Because a vacuum precludes the use of flowing media, an alternative method had to be developed to achieve uniform

kernel motion. The stated requirements were incorporated into a construction for moving the spheres on a stepped plate that was aligned parallel to the target and ensured conveyance of the spheres at a constant distance to the target through use of a pneumatically controlled lifting device.

Initial testing of the device shown in Figure 8 for coating the spherical particles was performed. Utilizing their elasticity (Young's modulus of the substrate material ZrO_2 = approx. 200 GPa [35]) and inertia, the spheres moved up the profiled conveyor plate raised at a lifting frequency of about 1 Hz, rolled down the sides, and were again accelerated to the top of the profiled plate in a renewed cycle. The orientation of the profiled plate at an angle of 45° to the base plate and hence parallel to the target enabled the spheres to be heated via a second laser beam (diode laser), which was transmitted into the chamber through the window above it (Figure 7). The setup using a diode laser for substrate heating had been successfully used for coating of planar substrates before [49]. The spacing between the target and the substrate was 45 mm, similar to that used for coating of planar substrates. The spheres were moved rhythmically, rotated about their central axes, and continuously coated.

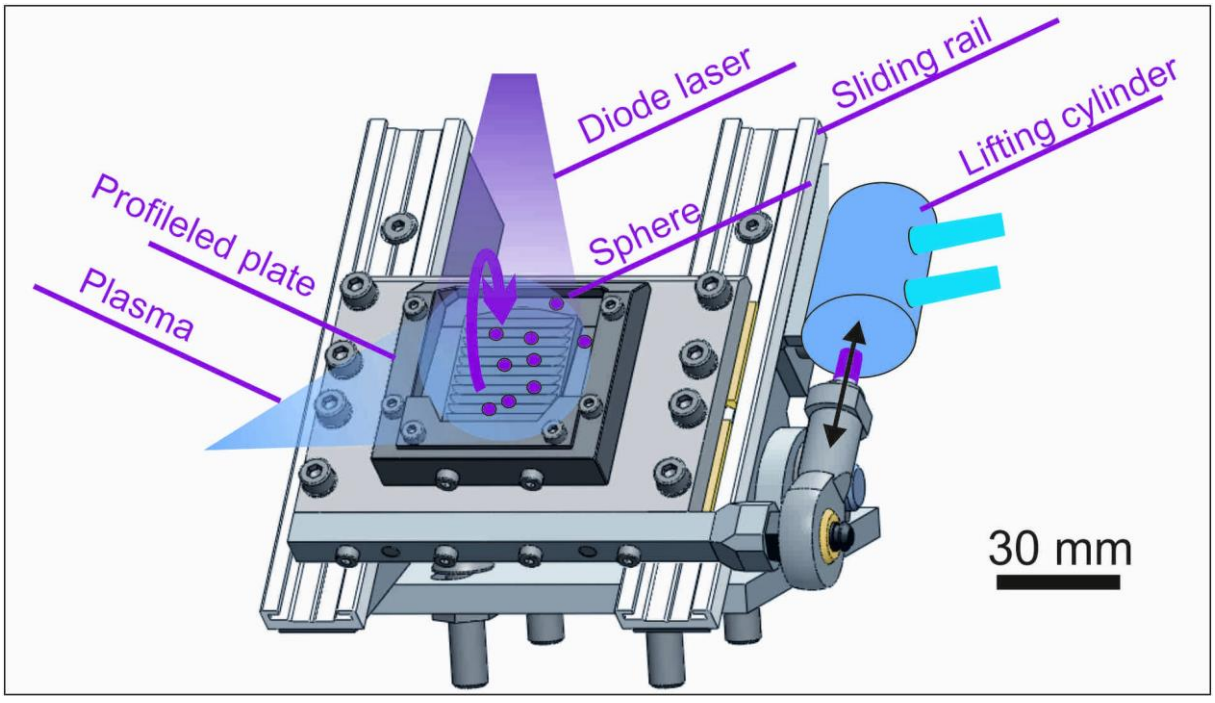


Figure 8: Sphere-conveying device

This holder proved to be suitable for generating thin coatings of thickness on the order of a micrometer (coating duration: ≤ 30 min). In contrast, for longer processing times for generating thicker coatings, the lifting cylinder frequently failed due to increased friction of the plungers in the lifting cylinders caused by thermal expansion and contamination of the

plungers during the coating process. Even when the moving parts were covered as a protection from the particle flux, the problem persisted. To address these findings, an alternative particle-moving device was developed (shown in Figure 9). The particles were in a graphite crucible oriented at a 10° angle, whereby the plate diameter of 10 mm corresponded to the diameter of the diode laser beam in this plane. The graphite plate was secured pointwise to an aluminum adapter, which was rotated uniformly at 25 rounds per minute by a water-cooled motor. The motor was the same as the one used for target rotation and exhibited stable operation during the coating tests.

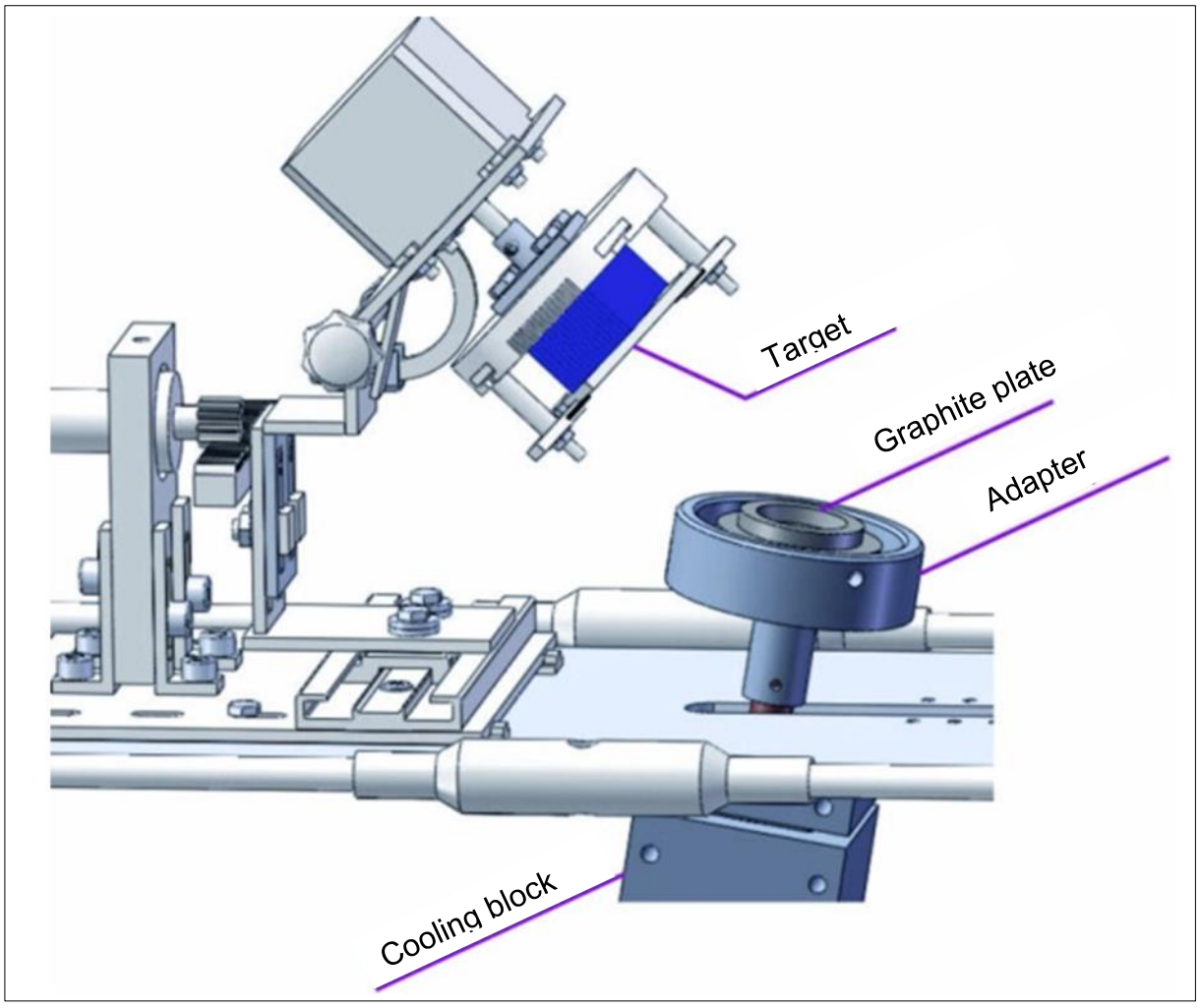


Figure 9: Modified holder for sphere coating

Comparison of a (planar) circular area and the surface of a sphere through the equation $\frac{\pi}{4}d^2 = k \cdot \pi d^2$ yielded a relationship k = 1/4, meaning that the deposition rate of spheres was expected to be only one-fourth of that of planar substrates. In the case of planar substrates, the coating rate was determined in the tests to be approximately 3 nm/s. Until a coating thickness of 10 µm on the surface of the sphere was reached (CVD coating was about 35 µm [36]), the deposition rate decreased continuously due to the accompanying

decrease in the transmission of the coupling window for the excimer laser. Measurements yielded an energy acting on the target Q_t of approx. 72% of the originally determined laser pulse energy Q_0. The reason for this was the secondary coating of the coupling window angled at 45° to the coating axis, although this coating was minimized through insertion of a screen and placement as far from the target as possible (distance: 400 mm). The time required to reach a specific coating thickness was empirically determined as:

$$t = v_{plate} \cdot s : T \tag{1.1}$$

where t was the coating time, v_{plate} the deposition rate on planar substrates, s the coating thickness, and T the transmission of the window. This approximation yielded a processing time of 5.1 hours for a coating thickness of 10 µm, which was confirmed experimentally. However, only the modified test setup shown in Figure 9 was suitable for conducting these lengthy coating tests.

4.3 Materials used

The coating tests were performed on alumina (Al_2O_3) and zirconia (ZrO_2) particles approx. 500 µm in diameter. According to the literature, these are the usual substrate materials used for investigating processes of diffusion of silver through SiC barrier coatings and served as a benchmark for comparison of the results. In addition, this work used optimized coating technology on spherical ZrO_2 substrates that were previously coated in a CVD process with a buffer layer and a pyrolytically deposited carbon coating at the University of Manchester to exhibit similar properties to those of TRISO particles.

As coating materials, i.e., targets, silver, silicon carbide (SiC), and boron carbide (B_4C) were used. The main properties of the substrate and target materials are summarized in Table 1 and Table 2.

Table 1: Physical properties of the target materials

	Silver *	SiC Target **	B_4C Target***
Density, gcm^{-3}	10.5	3.16	2.48
Melting temperature, °C	961.9	> 2300	
Coefficient of thermal expansion at 1000 °C, 10^{-6} K^{-1}	19.1 (20 °C)	5.2	6.3
Thermal conductivity, $W(mK)^{-1}$	429	125	36
Young's modulus at 20 °C, GPa	82.7	420	410
Poisson's ratio	0.367	0.17	0.18
Purity, %	99.99	99.9	> 99.0

*) Sputter target Ag Goodfellow GmbH, **) EKasic Fplus ESK Ceramics, ***) Kurt J. Lesker/htc-B_4C Ortwin Rave

Table 2: Physical properties of the substrate materials

	Spherical substrates	
	ZrO_2 *	Al_2O_3 **
Density, gcm^{-3}	6.0	3.71
Melting temperature, °C		2010
Coefficient of thermal expansion at 1000 °C, 10^{-6} K^{-1}	10.8	8.3
Thermal conductivity, $W(mK)^{-1}$	2	24
Young's modulus at 20 °C, GPa	210	330
Poisson's ratio		0.23
Surface roughness Ra, µm	0.01	220

*) Tosoh Corporation, **) Taimicron

Due to the different methods used to prepare them, the individual substrates exhibited different surface properties. The surface roughness is a significant factor in coatings because it determines whether the coating adheres to the substrate by (chemical or physical) adhesion only or additionally by mechanical anchoring [37]. The linear roughness R_a measurements listed in Table 2 fluctuated greatly among the spherical substrates. Micrographs of the substrate surfaces are shown in Figure 10 to Figure 12.

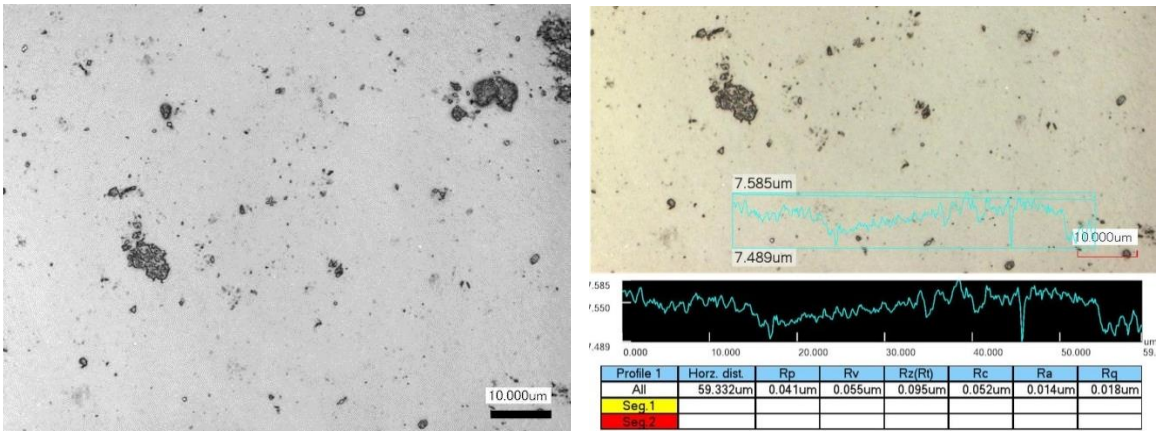


Figure 10: LSM surface and roughness of zirconia spheres (Ra = 14 nm)

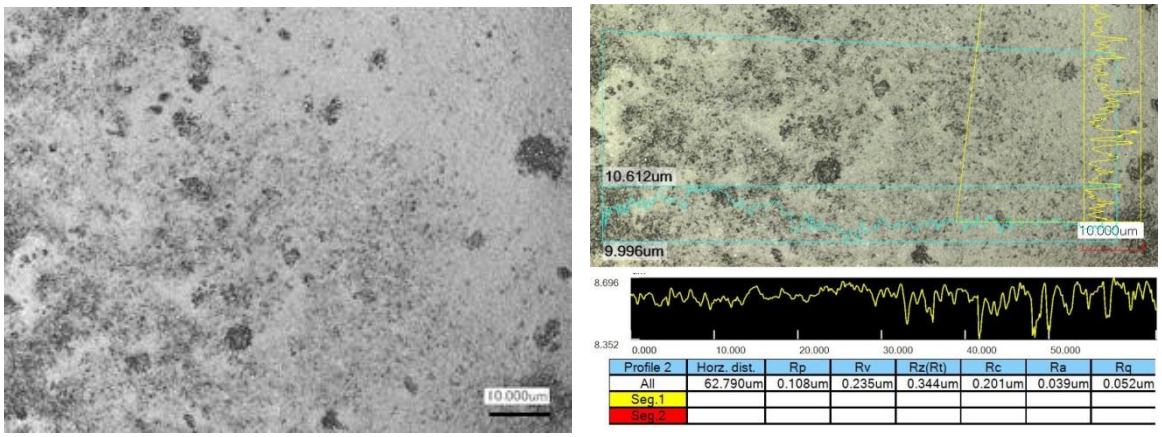


Figure 11: LSM surface and roughness of alumina spheres (Ra = 40 nm)

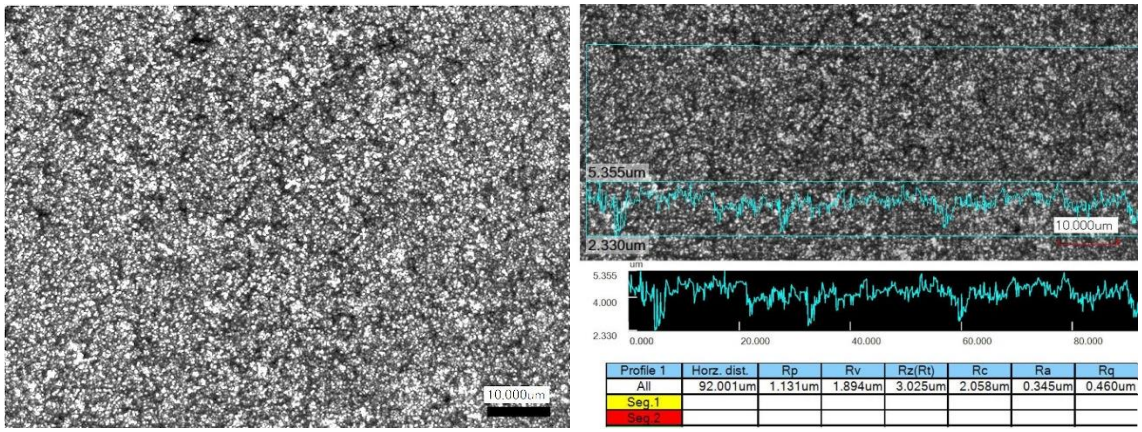


Figure 12: LSM surface and roughness of carbon-coated ZrO_2 spheres (Ra = 345 nm)

5 Results

5.1 Coating of ZrO_2 particles with silver

Coating with silver was performed at a pulse energy of 60 mJ, a pulse repetition frequency of 40 Hz, a coating time ranging from 5 to 15 min at room temperature, and a chamber pressure of 10^{-4} mbar. The resultant coating thickness was between 50 nm and 300 nm.

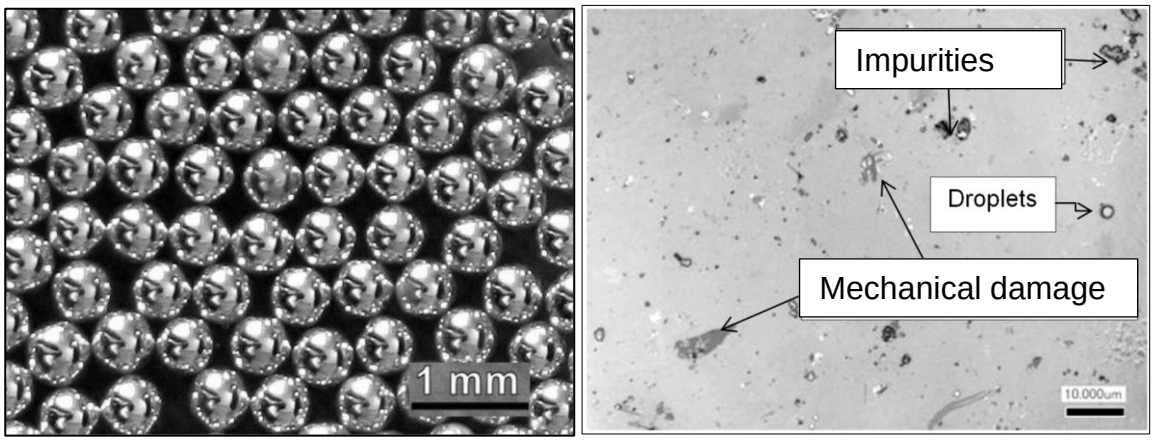


Figure 13: Photo of silver-coated spheres (left) and LSM micrograph of surface of silver coating (right) with typical impurities and mechanical damage

A photograph of coated particles and a LSM micrograph of the surface are shown in Figure 13. The micrograph shows typical impurities such as droplets, mechanical damage, and adhering contaminants. The number of droplets was found to increase with increasing pulse energy.

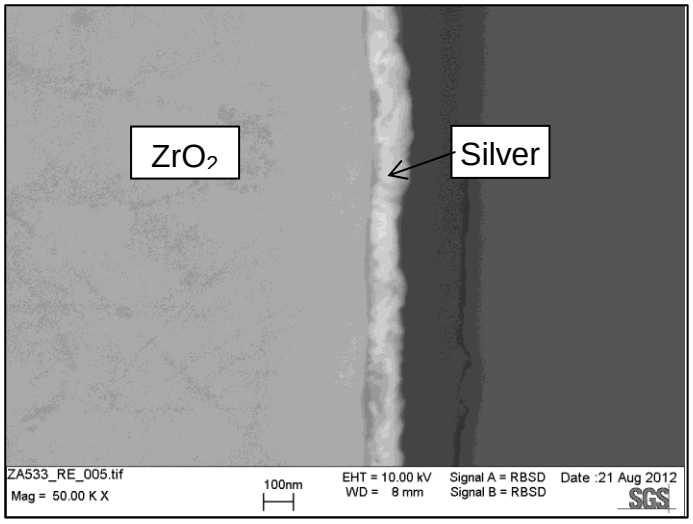


Figure 14: Cross section through a silver coating (SEM micrograph)

Figure 14 shows an SEM micrograph of a polished cross section through an approximately 100-nm-thick silver coating. The coating shows none of the pores or blowholes that would be expected with accumulation of particulates or droplets due to shadowing effects. The coating is homogeneous and adheres strongly to the substrate. The shadowing that can be observed in Figure 14 is presumably due to preparation artifacts. With these findings, it could be shown that silver, as an indicator for diffusion processes, could also easily be deposited onto spherical substrates.

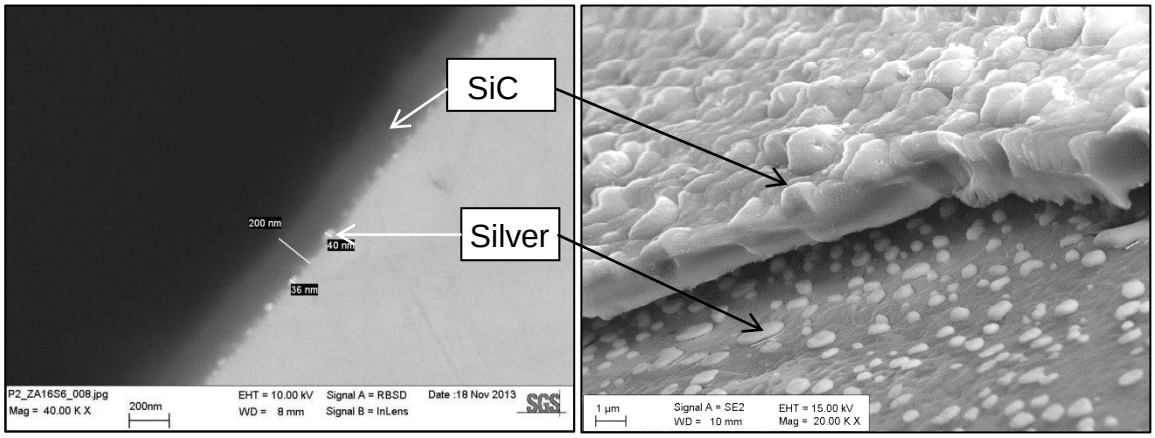


Figure 15: SEM micrographs of a UMAN polished cross section (left) and a fracture surface (right) of an approx. 50-nm-thick silver coating after SiC coating at 1000 °C with a chamber pressure of 10^{-1} mbar. The left figure was obtained by SEM analysis at JRC Petten.

Figure 15 shows a silver coating with an original thickness of about 50 nm after subsequent application of an additional SiC coating deposited at 1000 °C and a chamber pressure of 10^{-1} mbar. It can be seen that silver melted, formed fine beads, and solidified during deposition. No silver deposits can be detected in the SiC coating.

5.1.1 Coating of ZrO_2 particles with SiC on silver at room temperature

Coating with SiC on Ag was performed in the first step at room temperature in a high vacuum. With a pulse energy of 350 mJ and a pulse frequency of 40 Hz, it took about 58 min to generate spherical coatings comparable to those on the planar substrates (Figure 16).

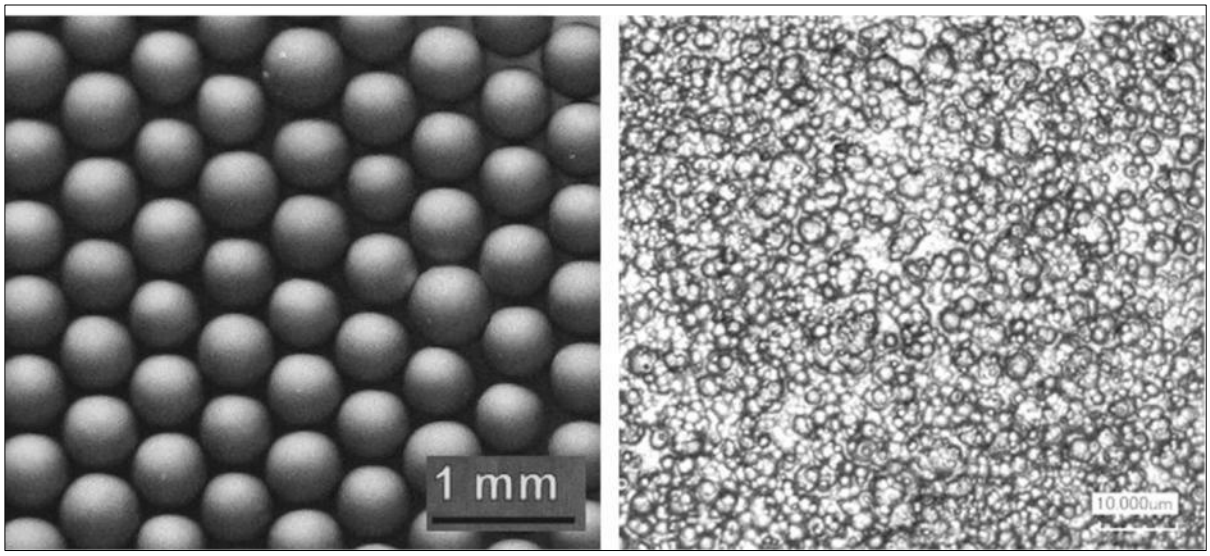


Figure 16: Coated ZrO_2 spheres mit 4-µm-thick SiC coatings on intermediate silver coatings: photograph (left) and LSM micrograph of specimen surface (right)

The thickness of this coating was approximately 4 µm. Crack-free and well-adhering coatings of thickness greater than 7 µm were also obtained. Thicker SiC coatings were not investigated. The surface structure (Figure 16) results neither from droplets nor from the roughness of the ZrO_2/Ag surface. The coatings deposited at room temperature exhibit inhomogeneities in the form of conical structures (Figure 17), which presumably lead to this surface structure. At higher deposition temperatures of between 350 °C and 600 °C, they were not observed to the same extent.

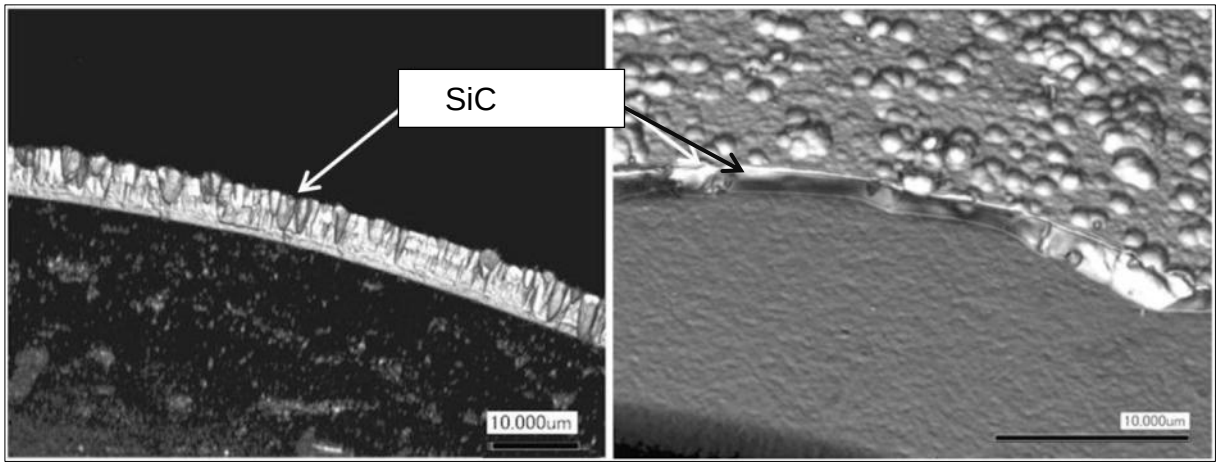


Figure 17: LSM micrographs of the fracture surface of an SiC coating at room temperature (left) and at > 350 °C (right)

The micrograph on the left in Figure 17 shows the fracture surface of an SiC shell, clearly showing these conical structures. The right micrograph, in contrast, shows the typical, glass-like fracture surface of amorphous SiC coatings, as is known from coating of planar

substrates ([43]). Of all spheres coated under these conditions, 97% exhibited dense interfaces between the ZrO_2 kernel, the silver coating, and the SiC coating.

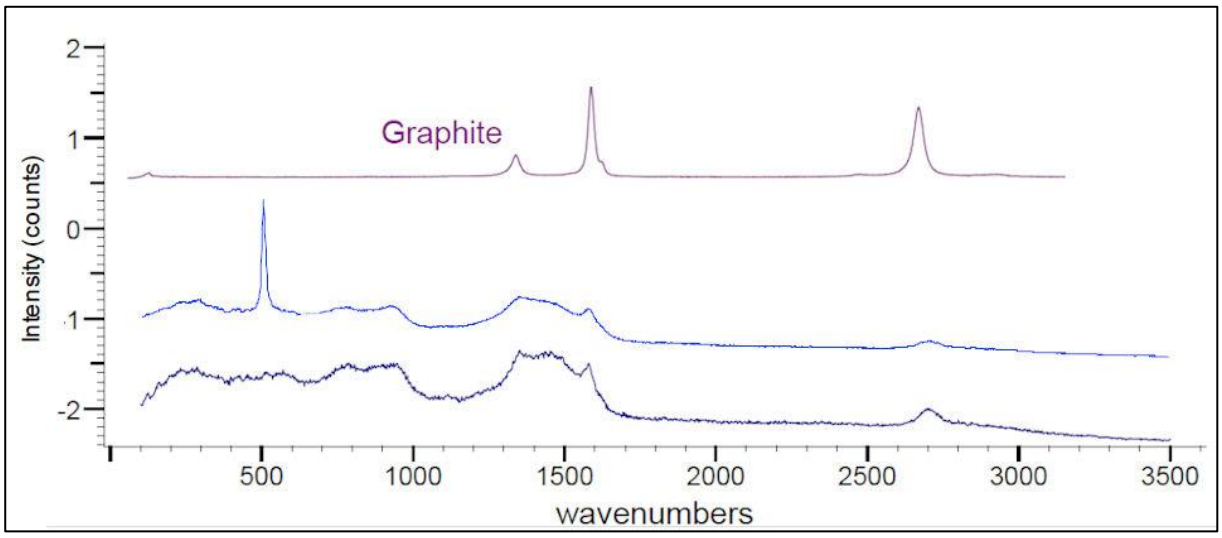


Figure 18: RAMAN spectra for a SiC coating deposited at room temperature

RAMAN spectra of these coatings, which were deposited at a temperature of less than 300 °C, are given in Figure 18. The two lower spectra represent typical measurement results, whereby the narrow peak at a wave number of 520 can clearly be assigned to silicon. Additional peaks in the regions corresponding to graphite (exemplified by the upper curve) point to amorphous carbon due to their broadness and low intensities. SiC was not found in any of its modifications. Deposition of SiC at substrate temperatures of less than 300 °C was shown to lead to the existence of the separate elements Si and C and not to the chemical compound SiC.

5.1.2 Coating with SiC on silver in the temperature range from 350 °C to 800 °C

For deposition of an approx. 5-µm-thick SiC coating onto silver at a temperature ranging from above 350 °C to approx. 800 °C, the extent of spalling of the layer was seen to coincide with the increase in temperature.

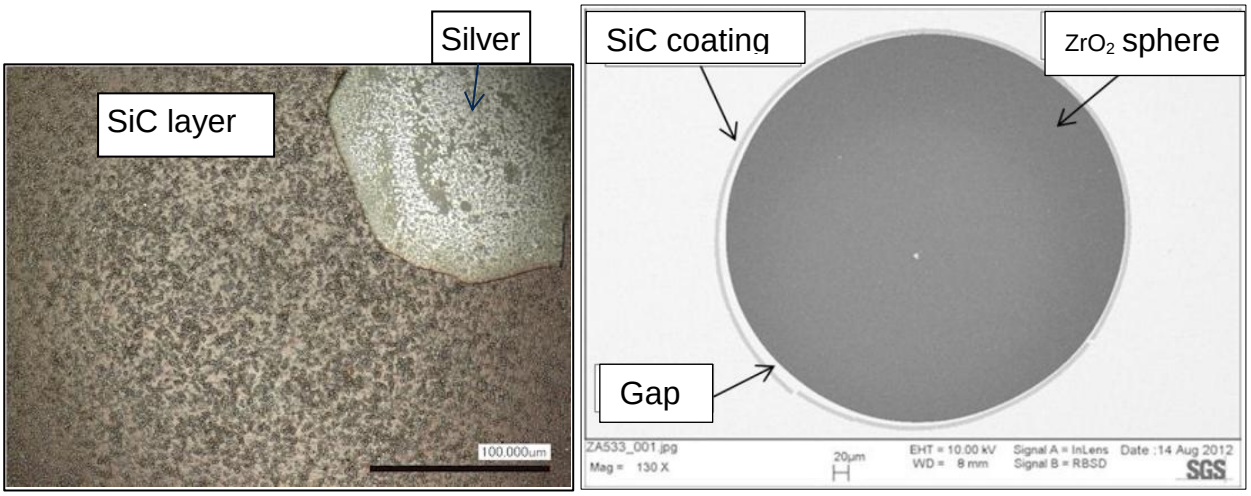


Figure 19: LSM micrograph of an SiC coating deposited onto silver at a temperature of about 700 °C in an argon atmosphere at 2.5 x 10^{-1} mbar, showing the typical spalling (left), and LM image of a cross section through an SiC coating under compressive stress with partial stress relief through crack formation (right)

Figure 19 shows an example of a slab that spalled off at a coating temperature of 700 °C due to a closed, web-like crack structure. The cross section to the right clearly shows that the SiC is mostly detached from the surface of the sphere. From the literature, it is known that for coating processes such as PLD with energetic particles, compressive stresses arise in the coating [44] [45]. A relationship between the substrate temperature and the increase in compressive stresses in the coating was found, with the slope starting off low at T_S = 600 °C and increasing steadily starting at a temperature of 800 °C. Zehnder et al. attributed this to densification of the crystalline coating structure and hence to a more pronounced effect of particles of high kinetic energy that became implanted in the coating [46]. The observation of stress-induced cracking with increasing coating temperature in the range between 350 °C and 800 °C was confirmed in the tests performed in this study.

X-ray photon spectroscopic investigations of the SiC coatings deposited at a temperature of greater than 350 °C yielded information about the coating compositions, as shown in Figure 20 for planar specimens.

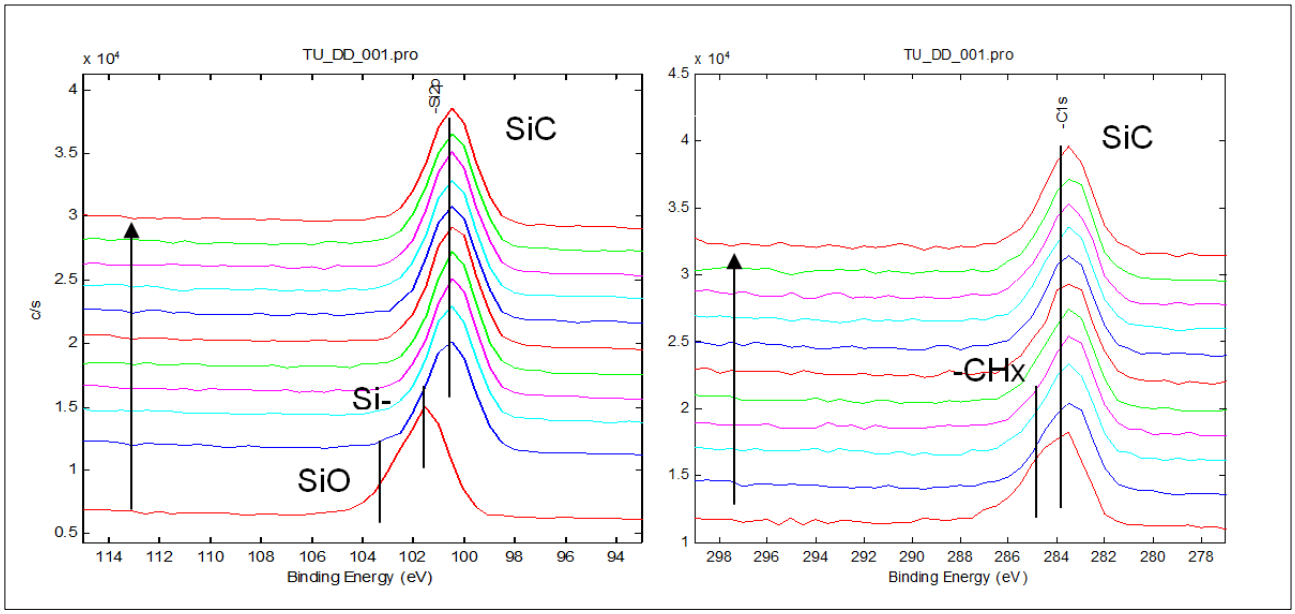


Figure 20: Results of XPS investigations of SiC coatings deposited at a temperature of greater than 350 °C for the region from the surface down to a depth of 50 nmFigure 20 illustrates the binding energies measured in the coatings. The ordinate indicates the sequence of sputtering cycles, with the maximum penetration depth being 50 nm. No changes were found at greater depths (> 10 nm). Primarily via the first two spectra, a shift in both the Si2p peak and the C1s peak, both of which were caused by near-surface reactions with reaction products SiO_2, SiO_x, and CH_x, was recorded. In contrast, starting at a depth of 10 nm, clear Si2p and C1s peaks were formed, providing evidence of a nearly stoichiometric SiC coating. Crystalline components of the coatings deposited at temperatures below 800 °C were precluded due to the crystallization temperature of ≥ 800 °C.

5.1.3 Coating of silver with SiC in the temperature range from 800 °C to 1000°C

Submicrometer-to-micrometer-thick SiC coatings on silver could not be deposited without cracking at a coating temperature of > 800 °C and a chamber pressure of 2.5 x 10^{-1} mbar. Tests performed at low temperatures (ca. 350 °C) for the first 15%–85% of the coating time and at higher temperatures for the remaining time (in a fine vacuum in both cases) also led to cracking of the coating. Tests performed at low temperatures (ca. 350 °C) for the first 15%–85% of the coating time in a high vacuum (4 x 10^{-4} mbar) and at higher temperatures for the remaining time in a fine vacuum (2.5 x 10^{-1} mbar) yielded significantly different results.

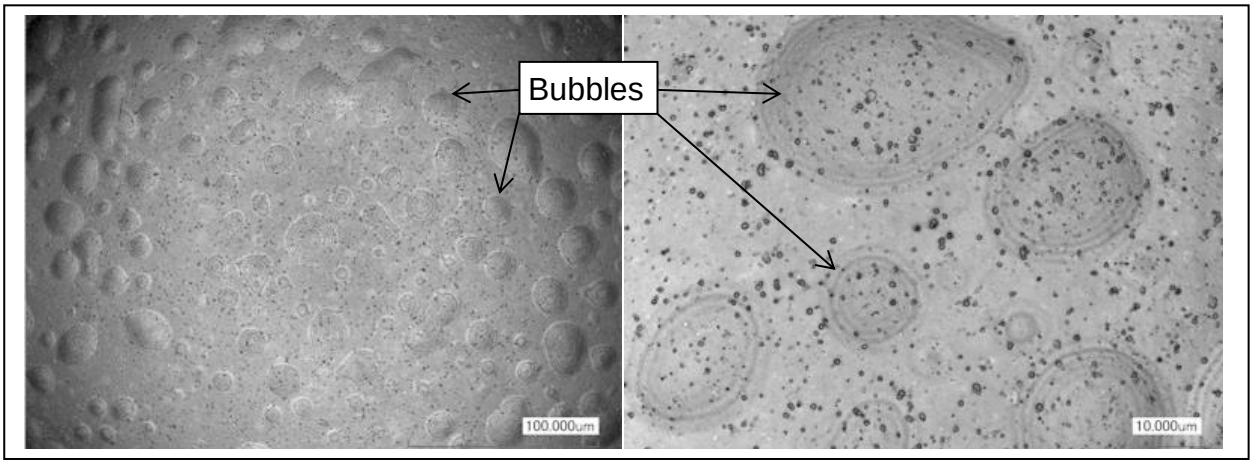


Figure 21: LSM micrographs of SiC coatings on silver with t1 = 10 min, T1 = 350 °C, and p1 = 10^{-4} mbar; and t2 = 2 min, T2 = 800 °C, and p2 = 10^{-1} mbar

Figure 21 shows a typical SiC coating of thickness ≤ 1 µm produced in two different pressure (high vacuum or fine vacuum) and temperature (< 800 °C or > 800 °C) regimes. Unlike the coatings deposited in a fine vacuum at comparable temperatures, these coatings did not show, or rarely showed, cracking. The coatings exhibited discrete buckled regions but otherwise exhibited good adhesion. It was not possible in this study to determine any influencing factors for the manifestation of the humps. For coating temperatures of about 1000 °C, cracks arose primarily at the hump boundaries, sometimes causing the buckled surfaces to detach, and were intertwined. The extent to which the coating leads to recrystallization of the underlying amorphous coating deposited at temperatures above 800 °C is not known.

In none of the coatings produced under the conditions described above could a crystalline phase be detected by XRD. EDX analysis of the coatings supplies possible reasons for this.

Table 3 lists the chemical compositions of the coatings deposited at various temperatures and pressures. The oxygen content of the coating is strikingly high and fluctuates strongly with changes in chamber pressure and temperature. The detection of oxygen can in principle be traced back to the significantly higher excitation depth for this light element. The silicon-to-carbon ratio decreases strongly with increasing chamber pressure and temperature. Under these circumstances, formation of a stoichiometric SiC phase is unlikely.

Table 3: Chemical compositions of coatings deposited at various temperatures

Pressure, mbar	10^{-4}	10^{-3}	10^{-4}, 10 min 10^{-1}, 5 min
Temperature, °C	25	800	900
Element, atom %			
C K	26.93	62.94	75
O K	47.93	11.42	25
Si K	25.13	25.64	12.5
Si/C	**0.93**	**0.41**	**0.16**

With knowledge of the coating composition, more tests were performed to determine the extent to which multiple purging of the chamber with argon to minimize the residual oxygen content changed the coating stoichiometry. In this test series, the ratio between low-temperature coating (at 350 °C) and high-temperature coating (at 800 °C) was changed from 5:1 (Figure 21) to 2.67:1 to recrystallize the amorphous structure. Coatings were deposited onto Al_2O_3 particles with the aim of determining whether or not the effect of different particle expansion behavior could help explain the occurrence of buckling.

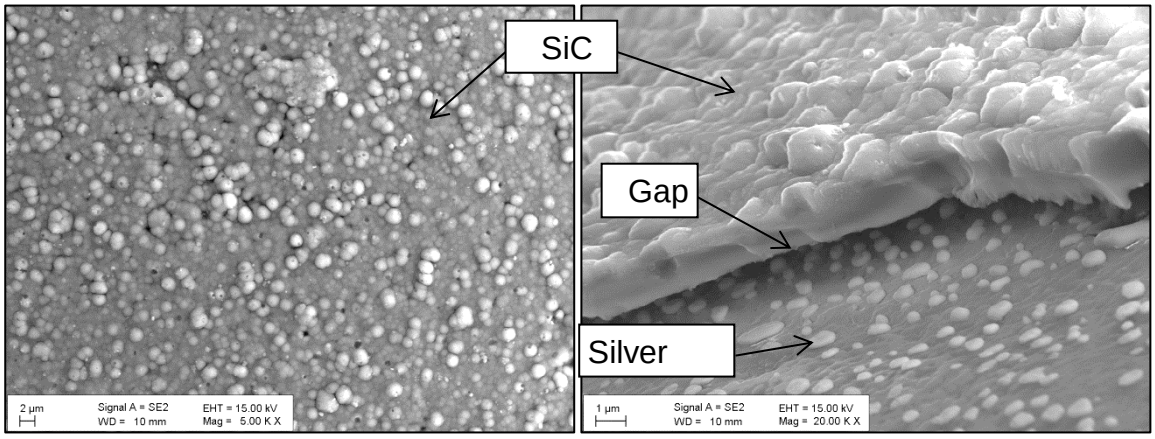


Figure 22: SEM micrographs (JRC-IET, Petten) of the surface of the SiC coating (left) and a cross section through the fracture surface of the coating on silver (right) for a coating thickness of 2 µm and Ra = 100 nm, with t1 = 40 min, T1 = 350 °C, and p1 = 10^{-4} mbar; and t2 = 15 min, T2 = 800 °C, and p2 = 10^{-1} mbar

Figure 22 presents coating surface micrographs. The coating surface appears to be homogeneous, highly densified, and free of cracks (cf. Figure 19 and Figure 21). Mechanical loading of the SiC coating leads to coating fracture and reveals the low adhesion to the substrate (right). The intermediate coating and the substrate exist side by side without being mechanically anchored or joined by adhesion or chemical bonding. In contrast to coating deposition onto ZrO_2 kernels, in this case, no buckling occurred.

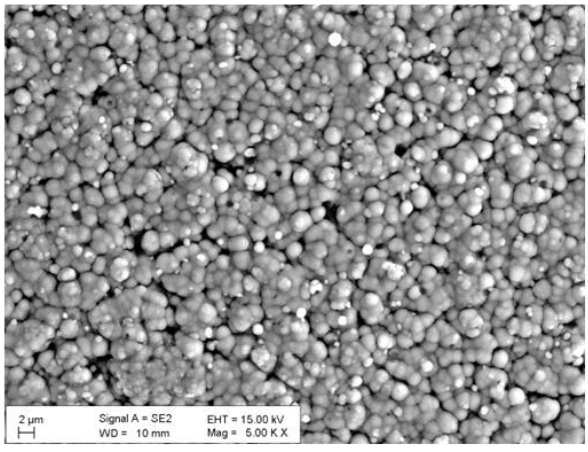
Table 4: Chemical compositions of the SiC coatings deposited onto silver after three argon purging cycles in the vacuum chamber for a coating thickness of 2 µm with t1 = 40 min, T1 = 350 °C, and p2 = 10^{-4} mbar; and t2 = 15 min, T2 = 800 °C, and p2 = 10^{-1} mbar (Results from JRC Petten).

	C	O	Si	Si/C
Atom %	40.16	18.73	41.11	**1.02**

Table 4 shows the results of EDX analysis. Increasing the purity of the working atmosphere resulted in a coating with a nearly stoichiometric ratio of Si:C of 1.02. Despite the coating temperature of 800 °C and the stoichiometric Si:C ratio, no crystalline SiC phases could be detected for a coating thickness of 2 µm.

5.2 Coating of carbon-covered ZrO_2 particles with silver and SiC

The extent to which the results of the silver-SiC coating systems deposited onto ZrO_2 could be transferred to the pyrolytically deposited carbon coating with different thermophysical properties was investigated. The University of Manchester supplied ZrO_2 kernels that were coated with porous carbon buffer layers deposited by CVD and dense pyrolytically deposited coatings (PyC layers) and had densities and carbon coating thicknesses similar to those of TRISO particles.



	C	O	Si	Si/C
Atom %	49.11	4.78	46.11	**0.94**

Figure 23: SEM micrograph (JRC-IET, Petten) of the surface of the SiC coating (left) and EDX analysis of the coating (right) for a coating thickness of approx. 3 µm and Ra = 250 nm, with t1 = 45 min, T1 = 350–500 °C, and p1= 10^{-4} mbar; and t2 = 45 min, T2 = 800 °C, and p2 = 10^{-1} mbar

The surface of the coating shown in Figure 23 exhibits a similar structure to that of the sample shown in Figure 22 coated under similar conditions. The greater contrast is indicative of a higher surface roughness, which was confirmed through measurements in the 3D laser scanning microscope. The roughness of the coated specimen was 250 nm (versus

100 nm based on the image given in Figure 22). This is due to the higher initial roughness Ra = 350 nm of the PyC coating. The coating shows no signs of cracking, delamination, or buckling, which are all associated with stresses or stress relief in the coatings.

A cross section through the fracture surface of the coating system is shown in Figure 24. The surface irregularities do not affect the density or homogeneity of the coating, which is firmly anchored to the carbon layer. The silver layer is clearly identifiable as an intense white, strongly reflecting region between the SiC coating and the carbon substrate. The silver also exhibited no bubble formation or delamination under the given temperature conditions. EDX analysis yielded an almost stoichiometric C/Si ratio of nearly 1 for the SiC coating.

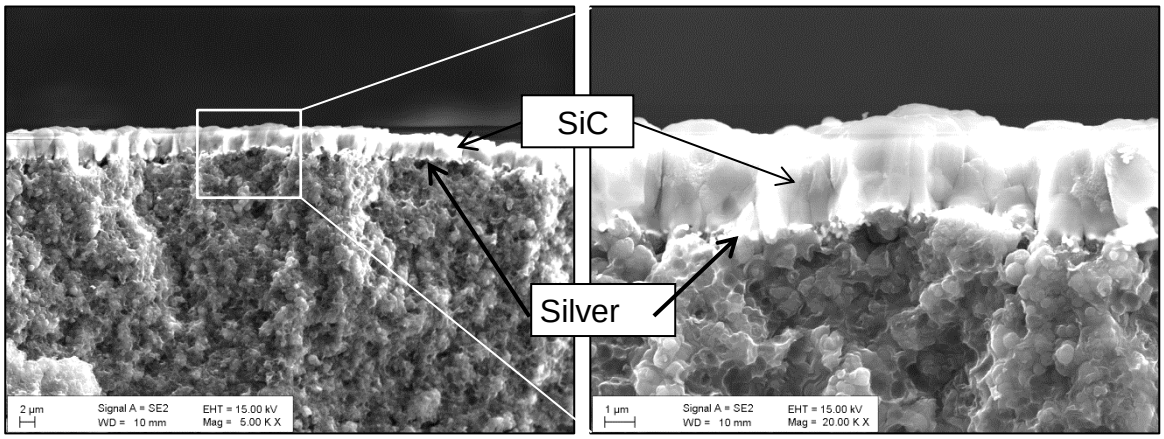


Figure 24: SEM micrographs (JRC-IET, Petten) of a cross section through the fracture surface of a PyC-silver-SiC coating system

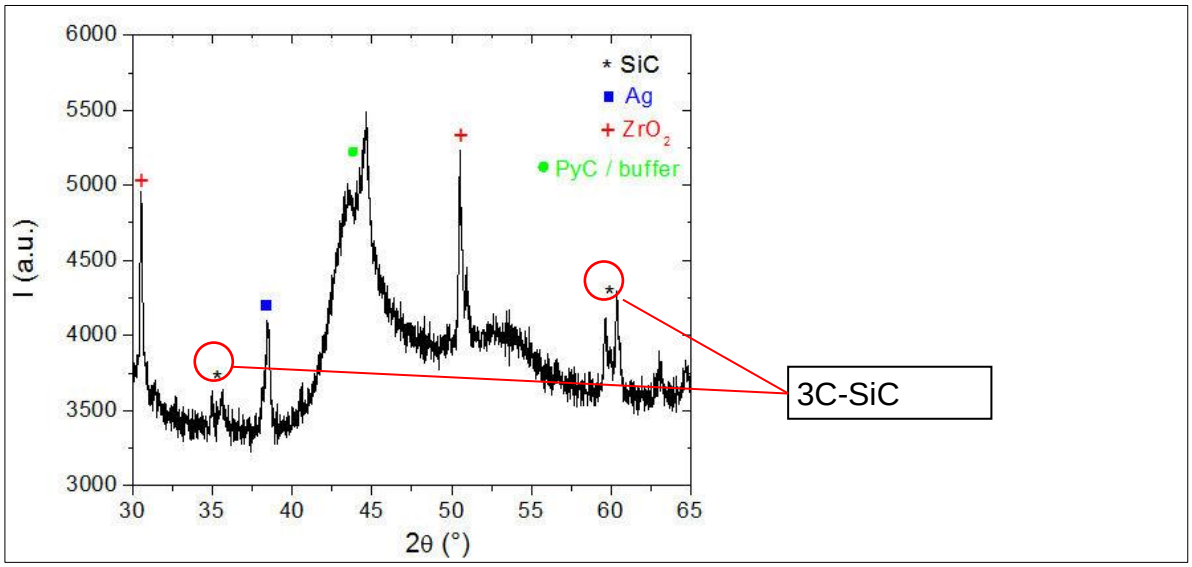


Figure 25: Grazing incidence X-ray diffraction pattern for a SiC-silver coating on PyC (JRC-IET Petten) with Tmax = 800 °C and a coating thickness of 3 µm

For these SiC-silver coating systems of thickness of about 3 µm deposited onto carbon at temperatures below 500 °C in a high vacuum for half of the total time and about 800 °C in an argon atmosphere for the remaining half of the time, crystalline components could be detected in the SiC coating. Figure 25 shows an XRD pattern in which the peaks of the CVD carbon coating, the ZrO_2 kernels, and the silver coating are clearly identifiable. Weaker, narrow peaks correspond to the crystalline phase of cubic SiC (3C-SiC) at 35.5° and evidently also at 60°. The relatively weak and broad peaks are indicative of a very fine crystalline structure with a grain size of a few nanometers.

5.3 Coating of Al_2O_3 particles with B_4C

5.3.1 Effect of porosity of the target material on coating quality

The first series of tests on PLD of B_4C coatings was performed with targets from the Kurt J. Lesker Company. A key property for the resultant coating is the density of the target material because it directly affects the formation of particulates and hence the density of the coating. For high-purity nonoxide target materials, density is a decisive quality criterion that results from sintering temperature, pressure, and time. If the extent of sintering is insufficient, detectable by the low ratio of actual to theoretical density, sintering necks have formed between adjacent crystallites and on thermal loading can break and lead to detachment of individual particles, which are then accelerated towards the substrate with the expanding plasma. After the importance of this target property was realized, coating was performed with a denser material from the company Rave.

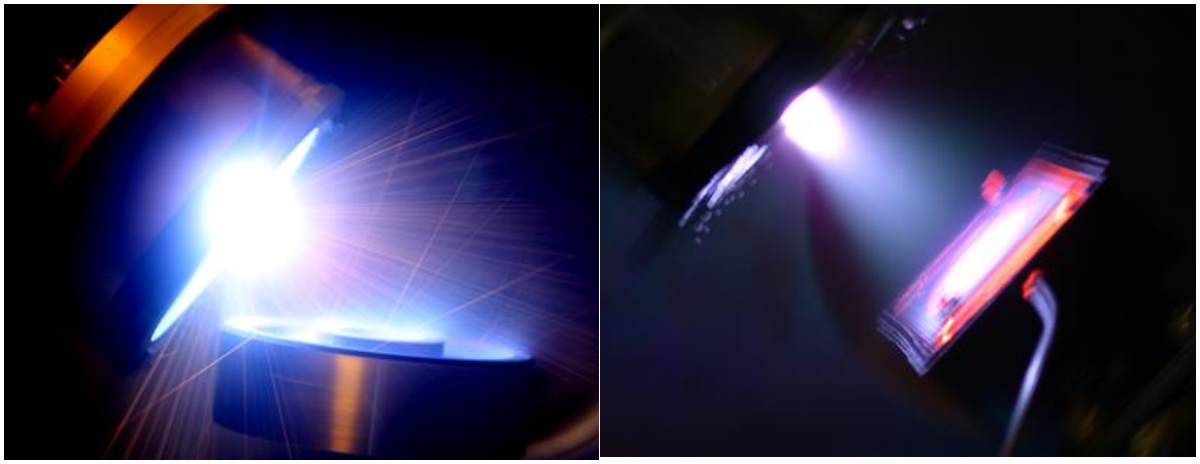


Figure 26: Appearance of plasma torch of a porous (left) and a dense (right) target

In the left image in Figure 26, an effect that can be attributed to insufficient sintering of the target from Lesker can be seen. Pure ablation of atoms, ions, electrons, and molecules is

shown on the right. Particles with sizes of about a micrometer already lead to easily recognizable spraying in the plasma torch.

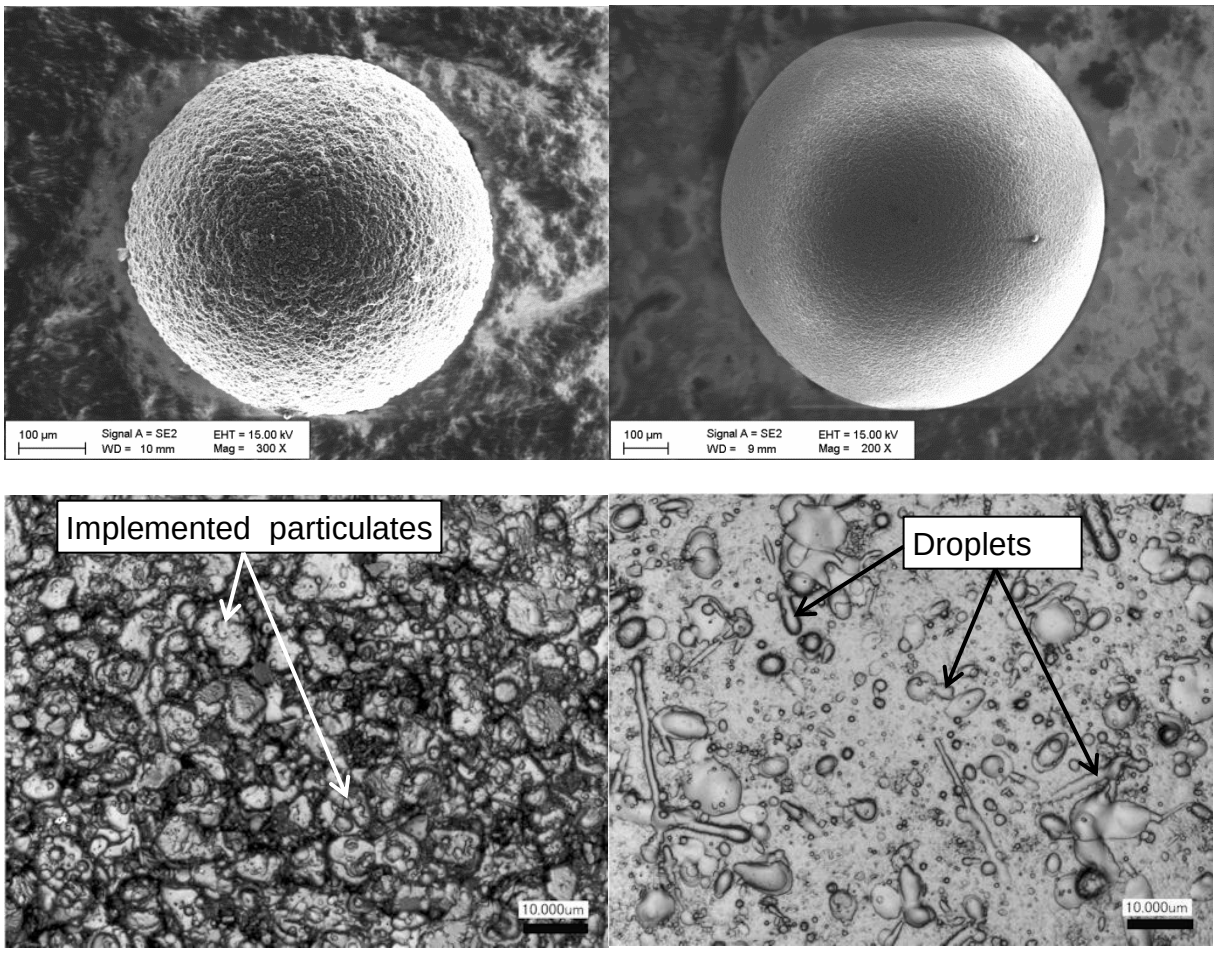


Figure 27: Effect of target quality on coating surface (left, Lesker: particulates lead to greater surface roughness; right, Rave: liquid phase-forming sintering additives increase the target density and hence the coating thickness; coating thickness in both cases: approx. 4 µm)

The effect of the different target qualities is illustrated by means of SEM micrographs of the overall structure in Figure 27 (top) and LSM micrographs of the surface (bottom). On the left, a coating that implemented particulates directly from the target nearly without a liquid phase and with a low droplet amount can be seen. The coating exhibits a “cauliflower-type” structure. There are no particulates detectable in the coating to the right, but splash-like droplets can be found with a dense distribution. The coating has a significantly lower roughness. A target of nearly theoretical density and high purity would be optimal for the tests, but there was no such product available from any of the contacted suppliers.

5.3.2 Coating with B_4C at temperatures of less than 300 °C

The first series of tests on PLD of B_4C was used to determine the minimum coating temperature required to generate crystalline (rhombohedral) B_4C coatings of thickness ap-

proaching 25 µm. Through heating of the alumina particles in a diode laser beam defocused to the plate size and with a power of 8 W (I = 4.5 W/cm²), a temperature of nearly 300 °C could be attained.

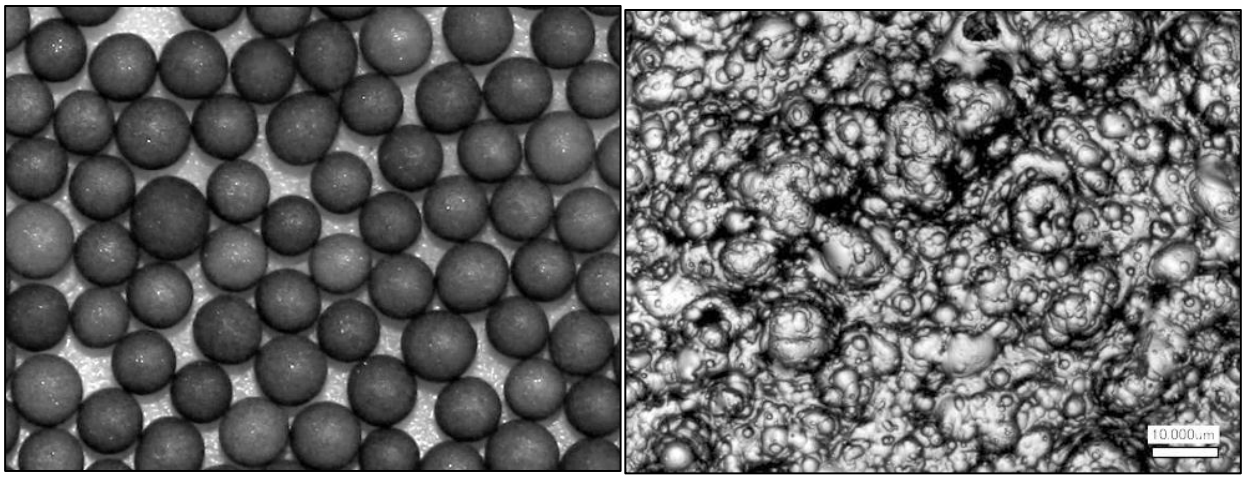


Figure 28: Photograph (left) and LSM micrograph (right) of coated Al_2O_3 spheres with B_4C coating of thickness 4 µm

Figure 28 shows a photograph of the spheres and an LSM micrograph of the surfaces of the spheres. An inhomogeneously structured coating surface of roughness Ra ~1 µm and Rz ~ 7.5 µm, which can primarily be traced back to the pronounced particulate formation when the Lesker target was used, can be observed.

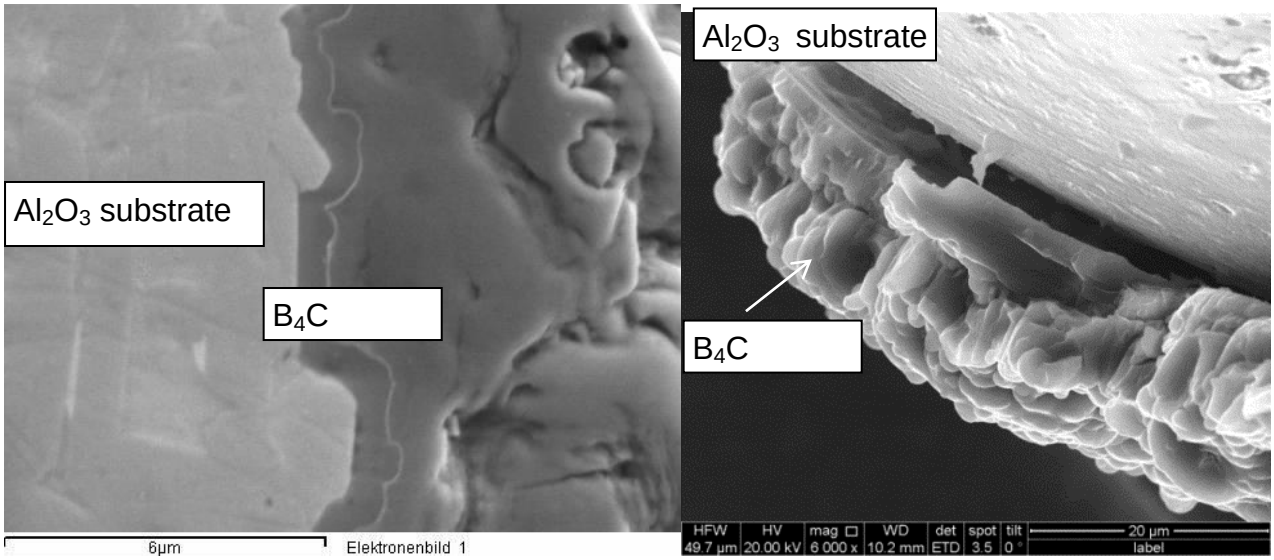


Figure 29: SEM micrographs of a cross section through a B_4C-coated sphere with coating thickness of approx. 5 µm (left) and a cross section through the fracture surface of a 17-µm-thick B_4C coating analyzed by UMAN (right) with use of a target from Lesker.

In Figure 29, a cross section through the interface between the coating and the substrate is shown; it appears to be pore-free, even in the vicinity of inhomogeneities that appear at right angles to the substrate surface. In the B_4C coating, pores arising from shadowing

effects in the region of deposited particulates can be detected. To the right, a fracture surface of a B_4C coating of thickness 17 µm deposited under the same conditions but for four times as long is shown. The coating is no longer adherent to the substrate surface, but instead it encloses the sphere like a loose shell. The coatings exhibit no cracks. Both porosity and a gap between the coating and the substrate impede the use of the B_4C coatings for the CPSTRESS irradiation experiments. Internal pressurization cannot be precisely controlled as helium can accumulate in not precisely defined hollow spaces. The porosity can be avoided through use of suitable targets, but in order for the internal coating stresses to be reduced, technological modifications are necessary. Minimization of the coating stresses may be achieved, for example, through inclusion of tempering cycles or by increasing the distance between the target and the substrate.

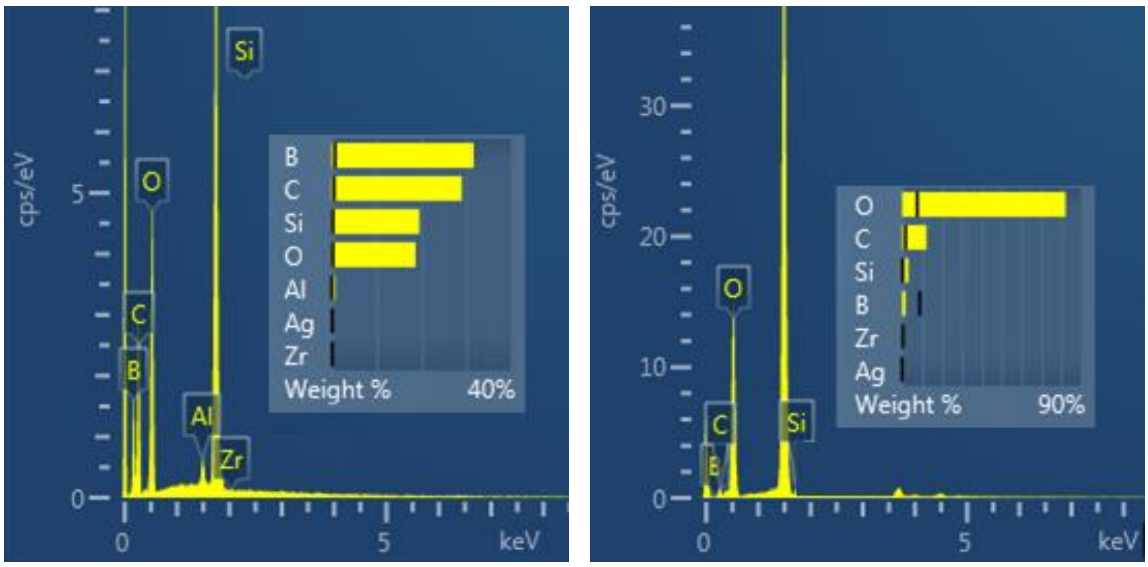


Figure 30: EDX analysis of B_4C coatings deposited at a temperature of < 300 °C after coating (left) and after heat treatment at 1600 °C (right)

The EDX analysis performed at University of Manchester (UMAN) shows the chemical compositions of the coatings as measured on the coating surfaces. These measurements on thin layers are technically very complicated and are often wrought with errors due to effects of the materials surrounding the bulb-shaped excitation region. Thus, they are only intended to indicate tendencies in this study. The silicon peaks in Figure 30 can be assigned to the specimen fixation and are not components of the coating. Especially the detection of the low-density element of oxygen can be attributed to an excitation depth that completely penetrates the Al_2O_3 spheres and hence enables signal reception from a measuring range that is more than 100 times larger. In the coating, a B:C ratio near 1 was measured (Mol_C: Mol_{B4C} = 1:1.2), significantly less than the stoichiometric ratio of 4:1.

The samples were heated in a furnace at 1600 °C at University of Manchester. After the coating was tempered, the EDX spectrum on the right was obtained. Boron and carbon were nearly no longer detectable. However, it is known from Gmelin's work [47] that even stoichiometric B_4C reacts very strongly with elements in main groups 4 to 6 at temperatures above 1000 °C. Detection of B_4C hence cannot be expected here.

5.3.3 Coating with B_4C at temperatures of between 300 °C and 700 °C

Increasing the beam power of the plate-sized defocused diode laser from 10 W (I = 6 W/cm²) to 24 W (I = 14 W/cm²) leads to heating of the particles to 300–1000 °C. According to Yan et al. [48], amorphous B_4C crystallizes in the range 300–850 °C, with crystalline B_4C having the highest temperature stability up to 2250 °C [47]. Deposition of nearly stoichiometric B_4C at a temperature of approx. 700 °C was successful, according to the results of EDX measurements at UMAN (Figure 31).

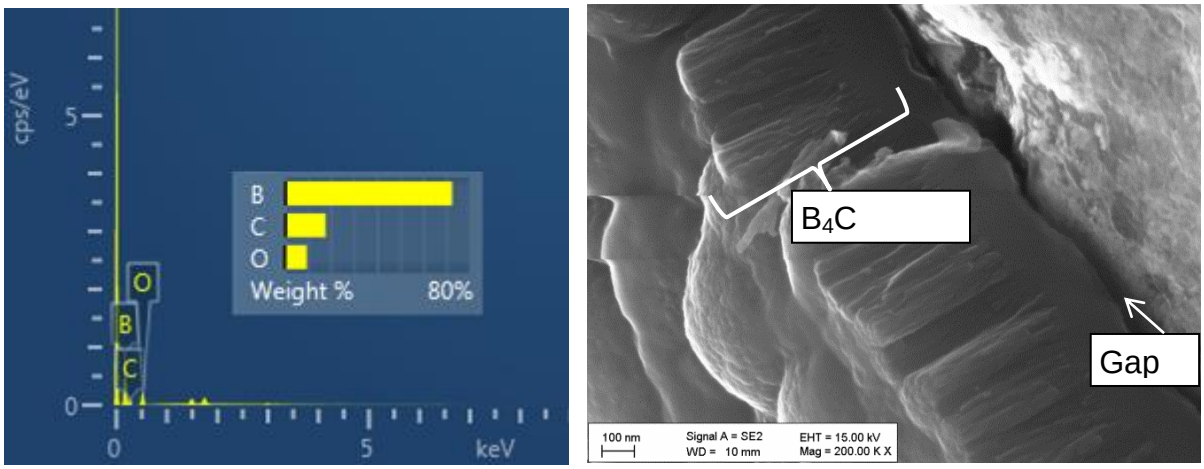


Figure 31: SEM-EDX analysis of a surface of a B_4C coating deposited at approx. 700 °C (UMAN) and microstructure of a 300-nm-thick coating (Petten) (right) for a target from Rave

For these samples, crystalline phases in the B_4C coatings were also detected.

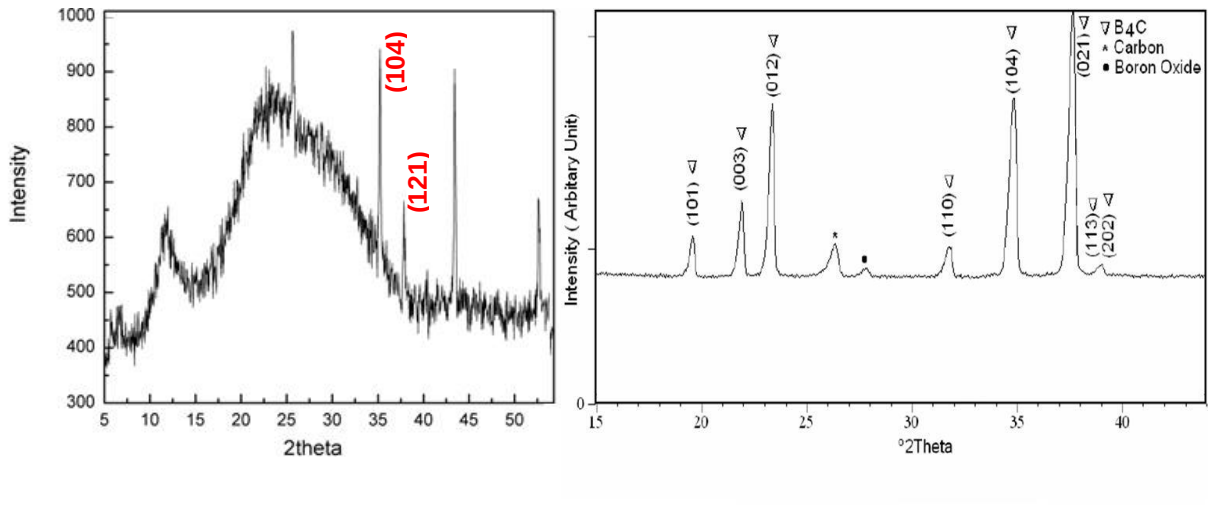


Figure 32: XRD spectra for the sample shown in Figure 31 and a B_4C reference specimen [49]

Apart from a predominant broad peak, indicative of amorphous regions, two main peaks of B_4C, (104) and (121), were detected (shown in spectrum to the right in Figure 32). A main peak of Al_2O_3 also occurred at 38° (021), making interpretation of these overlapping peaks difficult. To enable unequivocal identification of the crystalline B_4C phase and clear differentiation between the adjacent peaks of B_4C and Al_2O_3, it was necessary to coat B_4C on ZrO_2 particles of the same size. However, this was not successful.

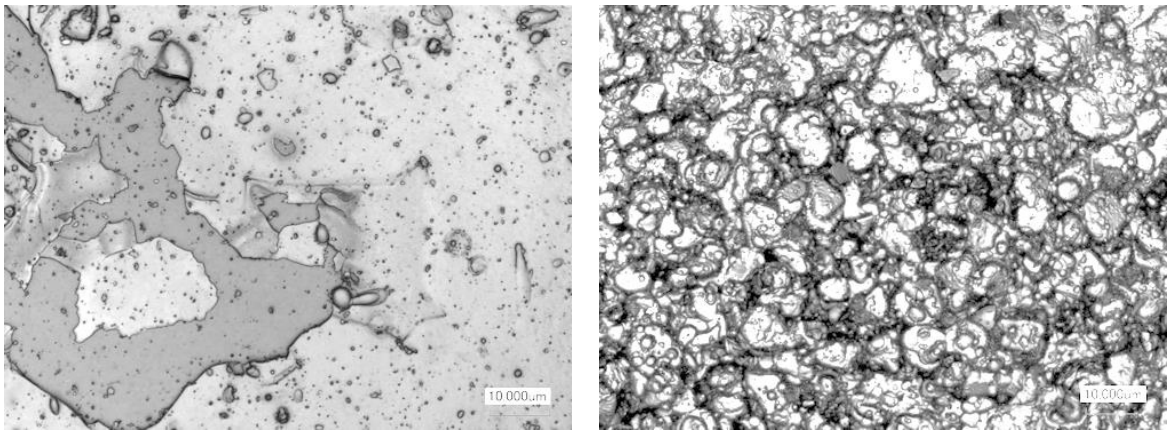


Figure 33: LSM micrographs of B_4C coating surfaces on ZrO_2 (left) and Al_2O_3 (right) with identical deposition conditions: Q= 270 mJ, f = 40 Hz, t = 70 min, T ~ 900 °C, and Rave target

In Figure 33, the effect of the substrate (ZrO_2 or Al_2O_3) on the resultant coating deposited under identical conditions is illustrated. On the ZrO_2 surface (left), the coating is only adhering to the substrate in isolated areas, large parts have been spalled off, and parts of the coating are only loosely enclosing the substrate without adhering to it. It is assumed that internal stresses in the coating due to the PLD process and the expansion behavior of ZrO_2 are responsible for the spalling. The thermal expansion coefficient of ZrO_2 (11 x 10^{-}

^{6} K^{-1}) is relatively high and comparable to those of metals. Additionally, at 1170 °C, a tetragonal-to-monoclinic phase transformation occurs with an accompanying volume change of up to 5%. The transformation is a diffusionless shear process occurring at a rate close to the speed of sound [50]. Even if the transformation temperature is higher than the measured temperature, a relationship is presumed due to inaccuracies in the temperature measurements and temperature inhomogeneities.

The micrograph to the right in Figure 31 clearly shows that the coating is no longer adhering to the substrate. Replacing the Lesker target with the denser target from Rave led to the desired denser coating (Figure 29, left). With the associated loss in porosity, however, internal stresses built up during the PLD process were not being compensated. This effect is known from earlier work on SiC coatings on planar substrates [51] and limited the maximum possible coating thickness to approx. 1 µm. Comparable results were obtained for coating with B_4C.

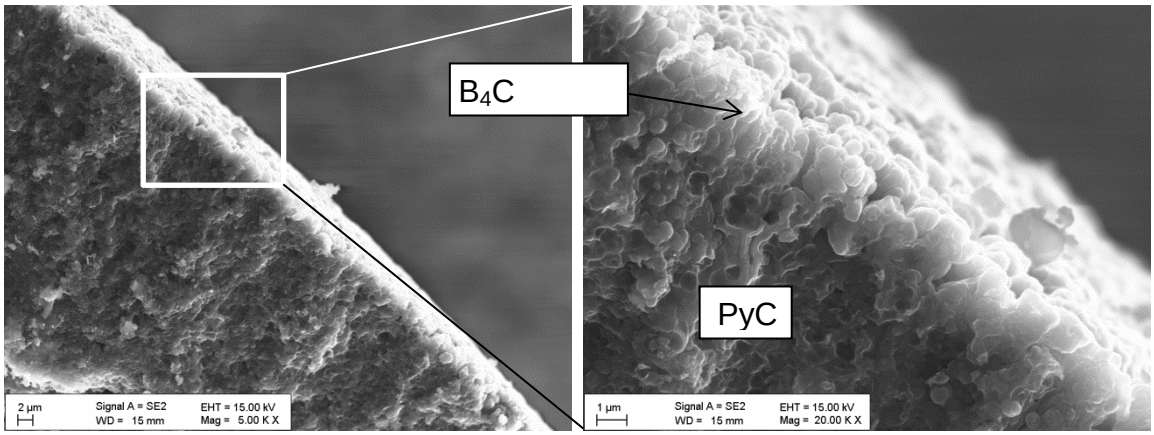


Figure 34: B_4C coating on pyrolytically deposited carbon (JRC-IET Petten)

Tests in which the temperature regime was varied in the range between 700 °C and 1000 °C with the aim of relieving the stresses were unsuccessful. Investigations based on the findings on coating of ZrO_2 spheres with SiC involving varying of the pressure conditions in the chamber (Section 5.1.3) have not yet been performed. The effect of the substrate material on the coating, or more specifically, on the stresses developing between the coating and the substrate, was also verified in these tests. Figure 34 shows a coating of thickness much greater than 1 µm and which exhibits a strongly adhering, crack-free, and uniform bond with the substrate.

6 Conclusions

Within the scope of the EU's ARCHER research project, the suitability of the PLD process for deposition of coatings or coating systems as components of the coating system for TRISO-coated particles was investigated to determine and quantify the coating integrity to prevent escape of radioactive fission products.

One aim of the work performed by TUD was to generate submicron-thick silver coatings on ZrO_2 particles to act as diffusion indicators, protected by thermally stable SiC coatings for subsequent CVD coating in a furnace at 1600 °C at the University of Manchester. For this purpose, a coating unit that uniformly moved the spheres to be coated in the vacuum chamber while maintaining their alignment to the target at a temperature of above 1000 °C for more than ten hours on a rotating graphite plate was successfully developed and tested.

Deposition of submicron-thick silver coatings was found to be easily possible. At a deposition rate of 0.5 nm/s, the coatings were nearly free of droplets and particulates. Under the given equipment-related conditions (pulse energy, pulse frequency, and vacuum level), the deposition rate could be increased to 3 nm/s. These coatings then primarily exhibited inhomogeneous coating thicknesses due to the presence of a large number of micron-sized droplets. The coatings were mainly free of cracks, adhered well to the substrate, and were dense. There were no signs of internal coating stresses.

Crystalline and hence thermally stable SiC coatings of thickness less than 1 µm could be generated in a high vacuum at deposition temperatures of ≥ 800 °C. Direct transfer of these results to silver-coated particles was hindered by the much less precise temperature measurement of the rotating spheres with a diameter < 1 mm and due to the use of higher chamber pressures. Crack-free high-temperature SiC coatings (≥ 800 °C) on silver were obtained through the combination of high-vacuum coating at temperatures of approximately 500 °C and a subsequent fine-vacuum coating at the crystallization temperature. These coatings were intact but exhibited bubbles. The ratio of silicon to carbon was significantly nonstoichiometric in some cases. Evacuation of the coating chamber and subsequent purging with 99.9999% argon three times yielded crack- and bubble-free coatings with a C/Si ratio approaching the stoichiometrice value of 1. Verfication of crystallinity in these low coating volumes was technically challenging. However, it can be concluded with certainty that these coatings exhibited nanocrystalline regions that could be assigned to cubic SiC.

A second objective of project partner TUD was to generate dense, well-adhering B_4C coatings on Al_2O_3 particles for use in the CPSTRESS experiments. Investigations were conducted to determine whether a coating thickness of 25 µm was achievable with the PLD process that is usually used for the generation of submicron-thick coatings.

Deposition of well-adhering, crystalline B_4C coatings of thickness reaching 6 µm was achieved at a deposition rate of 0.5 nm/s and a temperature above 700 °C. Below 700 °C, the B/C ratio in the coatings was strongly substoichiometric. Under these conditions, crack-free coatings with thicknesses of up to 17 µm could be produced. The increase in coating thickness, however, was accompanied by a loss in adhesion starting at a coating thickness of about 6 µm, probably due to the development of internal compressive stresses. The coating microstructures were porous.

It was found that the target quality, i.e., the degree of sintering, strongly affected the porosity of the resultant coating. With increasing degree of sintering of the target, the density of the deposited coating increased. The number of particulates originating from the target and deposited onto the substrate decreased, and the coating became more homogeneous. As the coating density increased, stresses were built up in the coating during the coating process, leading to spalling of the coating. The coating adhesion was strongly dependent on the substrate material. Among the investigated substrate materials ZrO_2, Al_2O_3, and graphite, graphite showed the highest adhesion. This could be explained by the fact that graphite had a lower coefficient of thermal expansion than that of B_4C, unlike the other substrate materials. The tensile stresses generated during cooling counteracted the internal compressive stresses.

Based on the findings obtained regarding coating of SiC on ZrO_2 and B_4C on Al_2O_3, it can be concluded that modification of the coating atmosphere can cause an increase in coating thickness and still retain the high adhesion and density of the coating.

7 References

[1] H.M. Smith, A.F. Turner, Vacuum deposited thin films using a ruby laser, *Appl. Opt*. 4, 147 (1965)

[2] D. Dijkkamp, T. Venkatesan, X.D. Wu at al., Preparation of Y-Ba-Cu oxide superconductor thin films using pulsed laser evaporation from high T_c bulk material, *Appl. Phys. Lett.* 51, 619 (1987)

[3] D.B. Chrisey, G.K. Hubler, Pulsed laser deposition of thin films, *Wiley New York,* 1994

[4] H. Muto, S. Kamiya, T. Kusumori, Groth mechanism of a-SiC hetero-epitaxioal films by PLD as studie od the laser photon, pulse- width and substrates dependence, Optical Materials 23 (2003) 43

[5] C. Ristoscu, G. Scol, C. Ghica at al., Femtosecuond pulse shaping for phase and morphology control in PLD: Synthesis of cubic SiC, *Applied Surface Science* 252 (2006) 4857–4862

[6] T. V. Vekantesan, *Laser Ablation*, Springer, Berlin (1994)

[7] G. Reiße and S. Weissmantel, "Pulsed Laser Deposition of Hexagonal and Cubic Boron Nitride Films," *Applied Physics A (Suppl.),* vol. 69, pp. S749-S753, 1999

[8] D. Rost, Laserpulsabscheidung von superharten Schichten auf der Basis von diamantartigem Kohlenstoff und kubischem Bornitrid, Dissertation der TU Ilmenau, 2008

[9] N. V. Lyanguzov, V. E. Kaidashev, V. B. Shirkokov et al.: Magnetron and Pulsed Laser Deposition of Silverand gold nanoparticles and discontinuous films and their optical properties, Technical Physics 57 (2012) 1411-1416

[10] H. Nakashima, Y. Sasaki, R. Osozawa et al.: Surface enhanced infrared absorption spectra on pulsed laser deposited silver island films, Thin Solid Films, 536 (2013) 166- 171

[11] T. Zehnder, A. Blatter, A. Bächli: SiC films prepared by pulsed excimer laser deposition, Thin Solid Films, 241 (1994) 138-141

[12] T. Sörènyi, R. Stuck, F. Antoni at. al: Number density and size distribution of droplets in KrF excimer laser deposited boron carbide films*, Applied Suface Science*, 2005, Vol. 247, Issues 1-4, page 45

[13] H. A. Castillo, E. Restrepo- Parra, J.M. Vèlez at. al: Substrate temperature influence on bron carbide coatings grown by the PLD technique, *Surface and Coatings Technology*, 2011, Vol. 205, Issue 12, Page 3607

[14] M. Diegel, F. Falk, R. Hergt, H. Hobert and H. Stafast**:** Crystalline SiC thin film deposition by laser ablation: influence of laser surface activation; *Applied Physics A: Materials Science & Processing*, 1998, Volume 66, Number 2, Pages 183-187

[15] J. S. Pelt, M. E. Ramsey, S. M. Durbin: Characterization of crystalline SiC films grown by pulsed laser deposition, Thin Solid Films 371 (2000) 72-79

[16] T. Kusumori, H. Muto, M. E. Brito: Contraol of polytoype formation in silicon carbide hereroepitaxial films by pulsed-laser deposition, Applied Physics Letters, 84, 8 (2004) 1272- 1274

[17] A. Keffous,K. Bourenane, M. Kechouane, at al.: Morphological, structural and optical properties of thin SiC layer growth onto silicon by pulsed laser deposition**;** *Vacuum*, Volume 81, Issue 5 (2007) 632

[18] F. Neri, F. Barreca, S. Trusso: Excimer laser ablation of silicon carbide ceramic targets; *Diamond and Related Materials*, Volume 11, Issue 2 (2002) 273

[19] Y.H Tang, T.-K. Sham, D. Yang, L. Xue Tang: Preparation and characterization of pulsed laser deposition (PLD) SiC films*; Applied Surface Science*, Volume 252, Issue 10, 15 March (2006) 3386

[20] M. Tabbal, A. Said, E. Hannoun et al.: Amorphous to crystalline phase transition in pulsed laser deposited silicon carbide, Applied Surface Sciende 253 (2007) 7050- 7059

[21] G. Monaco, D. Garoli, M. Natali et al.: Synthesis of heteroepiytaxial 3C-SiC by means of PLD, Applied Physics A (2011) 225-231

[22] A. Chauhan, W. Moran, S. Ge, at al: Pulsed laser deposition of silicon carbide on heat resistant materials; *Scripta Materialia*, Volume 52, Issue 8 (2005) 735

[23] M. Kracker, C. Worsch, C. Bocker et al.: Optical properties of dewetted thins silver/gold multilayer films on glass substrates, Thin Solid Films, 539 (2013) 47-54

[24] J.C. Alonso, R. Diamant, P. Castillo et al.: Thin films of silver nanoparticles depositied in vacuum by pulsed laser ablation using an YAG:Nd laser, Applied Surface Sciende, 255 (2009) 4933- 4937

[25] C.A. Smyth, I. Mirza, J.G. Lunney et al.: Surface-enhanced Raman spectroscopy (SERS) using Ag nanoparticle films produced by pulsed laser deposition, Applied Surface Science, 264 (2013), 31-35

[26] E. Fazio, F. Neri, P.M. Ossi et al.: Growth process of nanostructured silver films pused laser ablated in high-pressure inert gas, Applied Surface Science, 255 (2009), 9676-9679

[27] H. Nakashima, Y. Sasaki, R. Osozawa et al.: Surface enhanced infrared absorption spectra on pulsed laser deposited silver island films, Thin Solid Films, 536, (2013) 166-171

[28] P. DeVasConCellos, S. Bose, H. Heyenal et al.: Antimicrobial particulate silver coatings on stainless steel implants for fracture management, Materials Science and Engineering: C, 32, Issue 5 (2012) 1112-1120

[29] S. Svensson, F. Suska, L. Emanuelsson, A. Palmquist et al.: Osseointegration of titanium with an antimicrobial nanostructured noble metal, Nanomedicine; Nanotechnology, Biology and Medicine, 9, Issue 7 (2013) 1048-1056

[30] J. Podporska-Carroll, B. Quilty, R. Devery: Non-cytotoxic and antimicrobial plasma sprayed coatings for orthodaedic application, Materials Letters, 112 (2013) 54-57

[31] Young-Woo Lee et al.: Development of HTGR-coated particle fuel technology in Korea; Nuclear Engineering and Design 238 (2008) 2842-2853

[32] Hrovat, M., Schulten, R., Grosse, K-H.: Kugelförmiges Brennelement und dessen Herstellung für gasgekühlte Hochtemperatur-Kugelhaufen-Kernreaktoren (HTR); DE102006040309A1, 13.3.2008

[33] Charollais, F., Fonquernie, S. at al: CEA and AREVA R&D on htr fuel fabrication and presentation of the CAPRI experimental manufacturing line; Nuclear Engineering and Design 236 (2006) 534-542

[34] Reitano, R.; Baeri, P.; Marino, N.: Excimer laser induced thermal evaporation and ablation of silicon carbide, Applied Surface Science, 96-98 (1996) 302-308

[35] Informationszentrum Technische Keramik: Brevier Technische Keramik, Fahner Verlag 1999

[36] Lensa, W.: Internationale Entwicklungsprogramme zum Hochtemperaturreaktor.http://www.vdi.de/fileadmin/vdi_de/redakteur_dateien/get_dateien/Hochtemperaturreaktor-Fachvortrag.pdf 2007

[37] Hofmann, H.; Spindler, J.: Verfahren der Oberflächentechnik, Fachbuchverlag Leipzig, 2004

[38] Reflexionsgrad aus Wikipedia, der freien Enzyklopädie, de.wikipedia.org

[39] Shayan, A. R, Poyraz, H. P.: Laser Absorption for Si and SiC: https://www.wmich.edu/mfe/mrc/pdf/Amir%20and%20Bogac_Laser%20Absorption%20for%20Si%20and%20SiC_10-24-2008.pdf, Western Michigan University, 2008

[40] Gmelin, Handbook of Inorganic Chemistry, Si Sppl. Vol. B2 Compounds, Springer, 1984

[41] A. Anders, "A structure zone diagram including plasma-based deposition and ion etching," *Thin Solid Films,* vol. 518, pp. 4087-4090, 2010.

[42] D. Smith, Thin-Film Deposition - Principles and Practice, Library of Congress, 1995

[43] A.-M. Reinecke, M. Lustfeld, W. Lippmann, A. Hurtado: Creation of leak-proof silicon carbide diffusion barriers by means of pulsed laser deposition, Nuclear Engineering and Design, 271 (2014) 92-98

[44] C. Davis, "A simple model for the formation of compressive stress in thin films by ion bombardment," *Thin Solid Films,* vol. 226, pp. 30-34, 1993.

[45] R. Koch, "Stress in Evaporated and Sputtered Thin Films - A Comparison," *Surface & Coatings Technology,* vol. 204, pp. 1973-1982, 2010.

[46] T. Zehnder, A. Blatter and A. Bächli, "SiC films prepared by pulsed excimer laser deposition," *Thin Solid Films,* vol. 241, pp. 138-141, 1994.

[47] Gmelin, Handbook of Inorganic Chemistry, Boron Suppl. Vol. 2 Elemental Boron, Boron Carbides, Springer, 1981

[48] X.Q.Yan, W.Li, T. Goto at al., "Ramen spectroscopy of pressure-induced amophous boron carbide", Applied Physics Letters 88, 131905 (2006)

[49] Advances in Ceramics - Characterization, Raw Materials, Processing, Properties, Degradation and Healing, Edited by Costas Sikalidis, ISBN 978-953-307-504-4, 382 pages, Publisher: InTech, Chapters published August 01, 2011 under CC BY-NC-SA 3.0 license DOI: 10.5772/933

[50] S.C.M. Knoll, "Elektrophoretische Formgebung von nanoskaligem Zirkondioxid", Dissertationsschrift, Universität des Saarlandes, 2001

[51] A.-M. Reinecke, M. Lustfeld, W. Lippmann, A. Hurtado: Creation of leak-proof silicon carbide diffusion barriers by means of pulsed laser deposition, in: Nuclear Engineering and Design, vol. 271, pp. 92-98 (2014)